

Unsupervised anomaly detection in large-scale estuarine acoustic telemetry data

Siphendulwe Zaza^{1,2}, Marcellin Atemkeng^{1,2*}, Taryn S. Murray^{2,3}, John David Filmalter² and Paul D. Cowley²

¹Department of Mathematics, Rhodes University, PO Box 94, Makhanda, 6140, South Africa.

²South African Institute for Aquatic Biodiversity, Private Bag 1015, Makhanda, 6140, South Africa.

³Department of Ichthyology and Fisheries Science, Rhodes University, PO Box 94, Makhanda, 6140, South Africa.

*Correspondence: m.atemkeng@ru.ac.za.

Abstract

Acoustic telemetry data plays a vital role in understanding the behaviour and movement of aquatic animals. However, these datasets, which often consist of millions of individual data points, frequently contain anomalous movements that pose significant challenges. Traditionally, anomalous movements are identified either manually or through basic statistical methods, approaches that are time-consuming and prone to high rates of unidentified anomalies in large datasets. This study focuses on the development of automated classifiers for a large telemetry dataset comprising detections from fifty acoustically tagged dusky kob (*Argyrosomus japonicus*) monitored in the Breede Estuary, South Africa. Using an array of 16 acoustic receivers deployed throughout the estuary between 2016 and 2021, we collected over three million individual data points. We present detailed guidelines for data pre-processing, resampling strategies, labelling process, feature engineering, data splitting methodologies, and the selection and interpretation of machine learning and deep learning

models for anomaly detection. Among the evaluated models, neural networks autoencoder (NN-AE) demonstrated superior performance, aided by our proposed threshold-finding algorithm. NN-AE achieved a high recall with no false normal (i.e., no misclassifications of anomalous movements as normal patterns), a critical factor in ensuring that no true anomalies are overlooked. In contrast, other models exhibited false normal fractions exceeding 0.9, indicating they failed to detect the majority of true anomalies—a significant limitation for telemetry studies where undetected anomalies can distort interpretations of movement patterns. While the NN-AE's performance highlights its reliability and robustness in detecting anomalies, it faced challenges in accurately learning normal movement patterns when these patterns gradually deviated from anomalous ones. To the best of our knowledge, this study represents the first effort to develop automated methods leveraging machine learning and deep learning to address anomalous detections in acoustic telemetry data.

Keywords: Acoustic telemetry, *Argyrosomus japonicus*, machine learning, deep learning, Breede Estuary, dusky kob

1 Introduction

Studying fish movement and behaviour is crucial for understanding ecological dynamics and implementing effective conservation strategies [1, 2]. Movements can be studied using various methods, including conventional dart tags providing low-resolution, coarse-scale data [3], and acoustic telemetry which provides high-resolution, fine-scale data [4, 5]. Acoustic telemetry, which involves the recording of an acoustic signal released from an acoustic transmitter on a deployed acoustic receiver, is currently the most popular method for studying the movements of aquatic animals, providing valuable insights into their movements, habitat use, and survival [5, 6].

One of the biggest strengths of acoustic telemetry is the amount of data collected, which in some instances can reach millions of individual data points of numerous individuals from various species [7]. However, this is also one of its biggest challenges. Large datasets have their own difficulties when it comes to analyses [8]. Associated with (but not limited to) large datasets are anomalous or false detections [7, 8]. These anomalies can arise for various reasons, and occur as a result of a collision of acoustic transmissions which creates a detection of a different transmitter ID by the acoustic receiver [8]. These anomalies can significantly skew the interpretation of fish movements and behaviour patterns [8, 9], making it essential to develop a strong anomaly detection system to ensure data integrity. In smaller telemetry datasets, anomalies can often be identified visually after plotting the data. However, this method is far too time-consuming for larger datasets comprising millions of detections.

Several statistical packages have been developed that filter, process and analyse passive acoustic telemetry data in the statistical environment R [10], including *actel* [11], *rsp* [12], *telemetR* [13] and *ATfiltR* [7]. While each has its strengths, another option to process large quantities of detection data is through machine learning. Machine learning (ML) and deep learning (DL) models are increasingly being incorporated into biological studies. For example, automating the detection of Hainan gibbon *Nomascus hainanus* calls using deep neural networks, and monitoring population numbers of wildebeest and zebra using a U-Net-based deep learning model integrated with a post-processing clustering model [14]. In the aquatic environment, ML and DL models have been applied to underwater video analysis to detect atypical fish behaviour [15], and while their potential in acoustic telemetry remains relatively underexplored, these models are slowly being incorporated into telemetry studies. For example, the migration fate of Atlantic salmon *Salmo salar* smolts was classified using unsupervised k-means cluster analyses and supervised random forest models [16], predatory fishes have been identified through the use of predation tags and associated movements using random forest algorithms [17], relative habitat selection by multiple shark species was predicted using random forest models [18], and habitat suitability of two estuarine species was modeled using deep feed-forward Artificial Neural Networks [19].

Acoustic telemetry data, in essence, collects presence/absence data of tagged individuals. These data can be reduced to a time series, listing the dates and times tagged individuals (which have been tagged with acoustic transmitters that have unique ID codes) and the location at which the detections occurred. Traditional ML methods, such as Density-Based Spatial Clustering of Applications with Noise (DBSCAN), Local Outlier Factor (LOF), and Isolation Forest (IF), have been widely used to detect anomalies within time series data [20]. The effectiveness of DL approaches such as Neural Network Autoencoder (NN-AE) in detecting anomalies has also been shown [21]. However, a major limitation of traditional methods is their inability to capture complex temporal dependencies in time series data, which can lead to poor performance in certain scenarios [22]. In the context of big data, where traditional statistical methods may fall short, ML and DL classifiers, which can significantly improve the accuracy of false detections, offer a robust alternative for ensuring data integrity. This paper addresses the gap by detailing the training of ML and DL classifiers for the accurate identification of false detections of an important estuary-dependent species, dusky kob *Argyrosomus japonicus*, within a permanently open estuary along South Africa's southern coast. This paper aims to provide practitioners with a comprehensive understanding of the training process, the decision-making involved in model selection, and practical guidelines for these decisions.

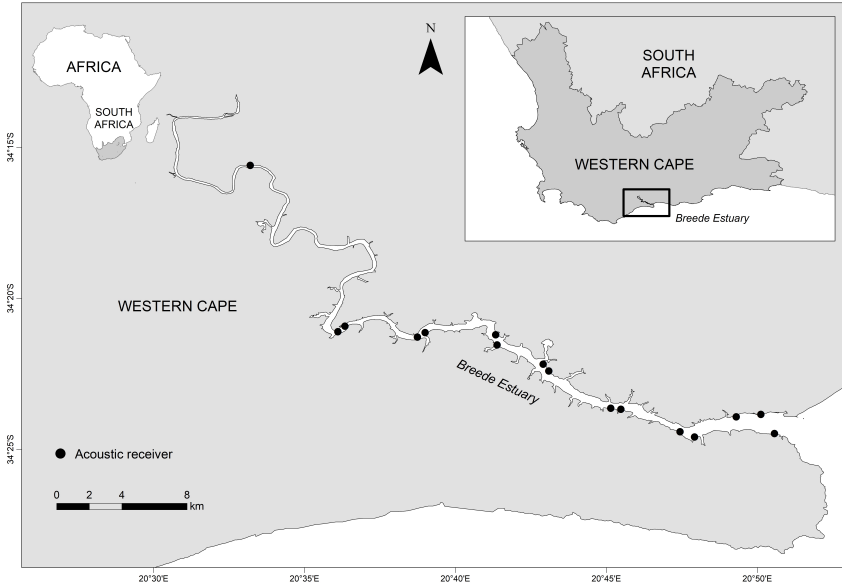


Figure 1 Map of the Breede Estuary showing the locations of acoustic receivers (black pins) deployed to monitor dusky kob movements in the estuary between 2016 and 2021.

2 Materials and methods

2.1 Study site and species

Fish were tagged in the large permanently open Breede Estuary situated in the Western Cape Province, South Africa (Figure 1). The estuary is 52 km in length and is a vital ecological and hydrological system that flows into the Indian Ocean at the coastal town of Witsand [23]. The Breede Estuary features diverse habitats like mudflats, channels, and intertidal zones, supporting a wide range of aquatic species, including several fish species of recreational and small-scale/subsistence importance [24], such as spotted grunter *Pomadasys commersonnii*, leervis *Lichia amia* and dusky kob [25].

The dusky kob is an important coastal fishery species with a South African distribution along the southeast coast from Cape Point to southern Mozambique (more abundant from Cape Agulhas to northern KwaZulu-Natal) [26]. Its life history is well known, with juveniles being dependent on estuaries as nursery habitats [27, 28], and even large adults remaining in estuaries for extended periods of time (up to seven or more years; ATAP, unpublished data). Their movements in South Africa have been well studied using acoustic telemetry [24, 29–31]. Juveniles are highly resident to estuaries [24, 29], and as adults (ATAP, unpublished data), making extensive use of these systems while in them [30]. Given the long-term residency to estuaries, and their

wide-scale use of most estuaries in which they occur (i.e. lower to upper reaches), acoustic telemetry data of dusky kob collected in estuaries form the ideal time series dataset for ML and DL model training.

2.2 Tagging and data collection

Between 2016 and 2021, 50 dusky kob, ranging in length from 660 to 1720 mm total length (TL) (average \pm SD: 1196 \pm 279 mm TL) were caught and tagged with individually coded acoustic transmitters (V16 transmitters, 69 kHz, Innovasea, Halifax, Canada) (Table 1). The tagging process involved catching fish using conventional rod and line techniques from a small boat or the bank of the estuary. Once caught, the fish was carefully pulled onto the boat, and placed into a flexible PVC sling, filled with water, and prepared for surgery. The head was covered with a cloth to reduce stress, and the gills remained submerged throughout the surgical procedure. The surgical procedure involved making a small incision (approximately 1.5 to 2 cm) in the fish's abdomen between the pelvic and anal fin, inserting the transmitter into the coelomic cavity, and then stitching the incision with two or three sutures. Once sutured, an antibacterial wound powder was placed over the incision site which congealed upon wetting. The surgical procedure followed that of [29]. Ethical approval was obtained from the South African Institute for Aquatic Biodiversity's Animal Ethics Committee (approval no. 2013_06), and research permits were obtained from the Department of Forestry, Fisheries and the Environment (permit no. RES2017/26, RES2019/16, RES2020/45).

The movements of the tagged dusky kob were monitored in the Breede Estuary between 2016 and 2021 using an array of 16 passive acoustic receivers (model VR2W, 69 kHz, Innovasea, Halifax, Canada) deployed throughout the estuary (Figure 1). Receivers were downloaded at least once a year to secure data using Innovasea's VUE software.

Overall, all 50 dusky kob were detected at least once, together accumulating 3013930 detections (Table 1). The average number of detections recorded per individual was 60278 (\pm 63276), ranging from 23 to 259676 detections, and individuals were detected for an average of 184 (\pm 217) days throughout the monitoring period, ranging from 2 to 1061 days (Table 1). The average number of detections recorded per day ranged from 11 to 854 average \pm SD: 336 \pm 128).

2.3 Data pre-processing

Prior to training ML and DL classifiers, several pre-processing steps were necessary, including cleaning the data to remove noise, normalising the data to ensure consistency, dealing with missing samples, and splitting the dataset into training, validation, and test sets for training and evaluation [32].

Table 1 Summary of tagging and acoustic monitoring details for dusky kob (*Argyrosomus japonicus*) in the Breede Estuary (2016-2021), showing total length, tagging date, detection count, station, and monitoring duration for each individual.

FishID	Total length (mm TL)	Tag date	No. of detections	No. of unique stations visited	No. of days detected
A69-9001-23701	1280	2015-11-01	71148	15	194
A69-9001-23702	990	2016-01-03	23	1	2
A69-9001-23668	1450	2016-10-05	42408	15	80
A69-9001-23669	1600	2016-10-15	67564	16	164
A69-9001-23670	1280	2016-10-16	88973	15	258
A69-9001-23671	1380	2016-10-16	76810	16	226
A69-9001-23672	1400	2016-10-17	8927	14	25
A69-9001-23728	1210	2016-10-17	73156	16	250
A69-9001-23727	1210	2016-10-18	12865	15	53
A69-9001-23726	1460	2016-10-18	27984	15	76
A69-9001-23737	1510	2016-10-18	84419	15	249
A69-9001-23738	1400	2016-10-18	7905	14	24
A69-9001-23739	1390	2016-10-18	57754	16	188
A69-9001-23747	1460	2016-10-18	86081	16	208
A69-9001-23745	1180	2016-10-19	33178	16	134
A69-9001-23746	1380	2016-10-19	25535	15	60
A69-9001-23748a	1140	2016-10-19	39614	15	123
A69-9001-23749	1290	2016-10-19	37648	15	100
A69-9001-23750	1239	2016-10-19	112064	16	276
A69-9001-23751	1270	2016-10-19	57073	15	137
A69-9001-23754a	1180	2016-10-20	14804	15	63
A69-9001-23754b	705	2018-08-10	422	3	23
A69-9001-23675b	750	2018-08-10	149205	15	542
A69-9001-23766b	1140	2016-10-20	55565	16	150
A69-9001-23753	1340	2016-10-20	29121	16	100
A69-9001-23697b	1230	2016-10-20	50402	15	122

2.4 Engineered features

Engineered features are a fundamental concept in ML and DL. They involve creating new features that are specifically informative for the task at hand, with the aim of improving the model’s performance [33]. In this study, new features were introduced to capture details not directly present in the data. These included “duration at the same station”, “number of detections”, “number of days detected”, “number of unique stations”, and “consecutive missing stations” (Table 2). The feature “duration at the same station” was of crucial importance as it identified cases where a fish was recorded at only one station during the entire study, possibly indicating a malfunction of the tag or a mortality. The “number of detections” and “number of days recorded” features provided information about the fish’s activity level and habitat use. The feature “number of unique stations” provided information about the spatial extent of the fish movements, and “consecutive missing stations” indicated possible gaps in the movements. Additionally, the feature “distance

Table 1 Cont.

FishID	Total length (mm TL)	Tag date	No. of detections	No. of unique stations visited	No. of days detected
A69-9001-23698b	1210	2016-10-29	41306	15	112
A69-9001-23682b	1140	2016-10-29	15749	15	45
A69-9001-50373b	1290	2016-10-29	10480	15	54
A69-9001-23774	1490	2016-10-29	13504	12	28
A69-9001-23741b	1310	2016-10-29	80670	14	212
A69-9001-23721	1230	2016-11-02	56559	16	193
A69-9001-23722	1190	2016-11-02	259676	1	1061
A69-9001-23723a	1340	2016-11-02	9837	15	34
A69-9001-23777	1190	2016-11-02	15067	13	54
A69-9001-23778	1190	2016-11-02	29839	16	126
A69-9001-23779	1160	2016-11-02	4461	11	18
A69-9001-23775a	1240	2016-11-02	57840	16	216
A69-9001-23724	1460	2016-11-11	2567	11	10
A69-9001-23732	1720	2017-04-12	127797	16	247
A69-9001-23769	1650	2017-05-05	4271	3	5
A69-9001-23730	1220	2017-02-24	8094	15	31
A69-9001-23858a	695	2017-08-25	239874	16	461
A69-9001-23859a	660	2017-08-25	17679	15	63
A69-9001-23860a	665	2017-08-26	214246	15	561
A69-9001-23861a	660	2017-08-30	44924	10	135
A69-9001-23862	680	2017-09-19	225462	16	953
A69-9001-23714a	700	2017-11-28	16364	9	37
A69-9001-23684b	695	2018-03-29	96051	15	484
A69-9001-23733	665	2018-09-20	110965	14	251

travelled” was introduced to quantify the spatial movement, which was previously unspecified. The distance feature, for example, was calculated using the Haversine formula to determine the great-circle distance between two geographic points. According to [34], the Haversine formula is defined as follows:

$$d = 2r \cdot \arcsin \sqrt{\sin^2 \left(\frac{\varphi_B - \varphi_A}{2} \right) + \cos(\varphi_A) \cdot \cos(\varphi_B) \cdot \sin^2 \left(\frac{\lambda_B - \lambda_A}{2} \right)}, \quad (1)$$

where φ_A and φ_B represent the latitudes, λ_A and λ_B represent the longitudes, r represents the radius of the sphere and d is the distance between the points.

2.5 Labelling process

A detailed labelling process was first required to prepare the data for effective anomaly detection. The labelling process was based on three primary criteria, each capturing different patterns of abnormal fish movement.

- *If an individual fish was recorded at only one station throughout the study period, then it was flagged as an anomaly:* This criterion identifies anomalies where

Table 2 Description of original and engineered features in the telemetry dataset comprising acoustic detections of dusky kob *Argyrosomus japonicus* tagged and monitored in the Breede Estuary, South Africa.

Feature description	
Original Features	
fishid	ID code of each individual animal.
receiver	The serial number of a specific receiver.
station	Name of the station.
lat	Geographic coordinate that indicates the north-south position of a fish location.
lon	Geographic coordinate that specifies the east-west position of a fish location.
date	The date on which an individual fish was detected.
time_sa	The time (UTC+2) at which an individual fish was detected.
Engineered Features	
distance	The distance between two points on the Earth's surface using the Haversine formula.
duration in same station	The time a fish remained at the same station before moving to another station or going undetected.
num detections	The total number of times a fish was detected during the study period.
num days detected	The number of separate days on which a fish was detected in the Breede Estuary.
num unique stations	The number of different stations on which a fish was detected throughout the Study period.
consecutive missing stations	A count of the number of consecutive stations that did not detect a fish, indicating periods when the fish moved out of detection range or through areas without receiver coverage.

an individual fish was detected exclusively at a single station throughout the entire observation period (Figure 2). While dusky kob have been recorded remaining stationary for a number of days at a time [30], not moving at all would suggest either natural or fishing mortality, where a tagged fish has been caught and the tag discarded within the vicinity of an acoustic receiver, and as such, an anomaly.

- *If an individual moves as per normal, but then remains in the vicinity of the same station for more than 120 days:* This criterion flags anomalies where a fish, after initially moving between stations as expected, remains at one station for more than 120 days. This prolonged stay suggests natural or fishing mortality, similar to Criterion 1.
- *If an individual fish is not detected by consecutive stations, but is missed by more than one consecutive station:* This criterion captures anomalies where a fish is not detected at consecutive stations (missed by more than one consecutive station) (Figure 3), which could suggest code collision resulting in the creation of false or anomalous detections. Alternatively, this might suggest that the fish may have moved past the receiver at a time when reception range was reduced, preventing detection. This can occur during periods of high environmental noise caused by strong winds, currents, or high levels of boat traffic, for example.

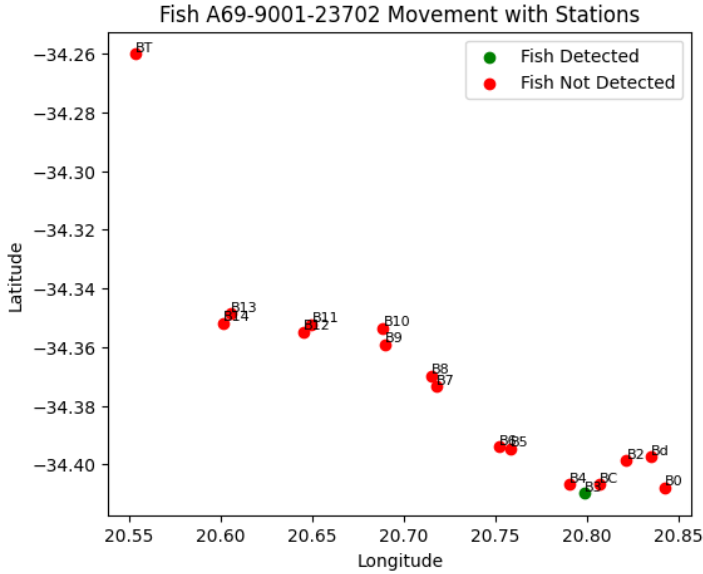


Figure 2 Patterns of detection for dusky kob A69-9001-23702 as an example of an anomalous detection pattern where a fish was only detected at one station, suggesting it remained stationary throughout the study period.

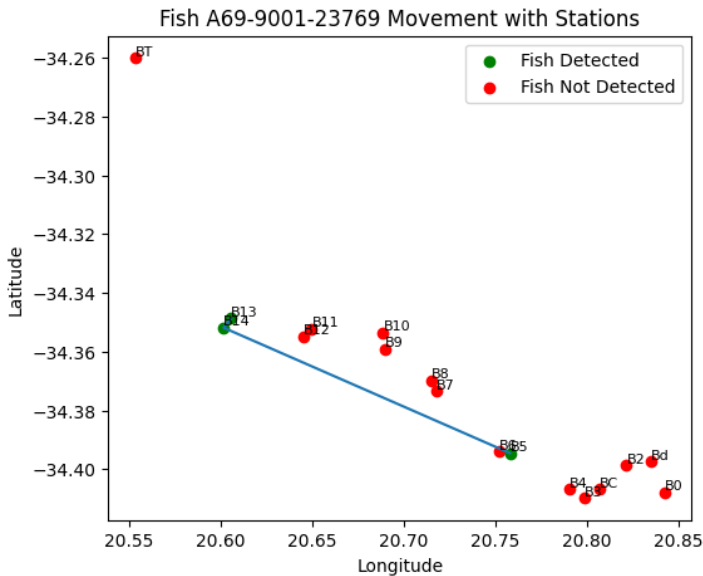


Figure 3 An example of an anomalous detection pattern, where dusky kob A69-9001-23769 was only detected at three out of 16 stations in the estuary, but not in a consecutive manner. This pattern deviates from the defined notion of normality, as the fish was missed by multiple consecutive stations, flagging it as an anomaly.

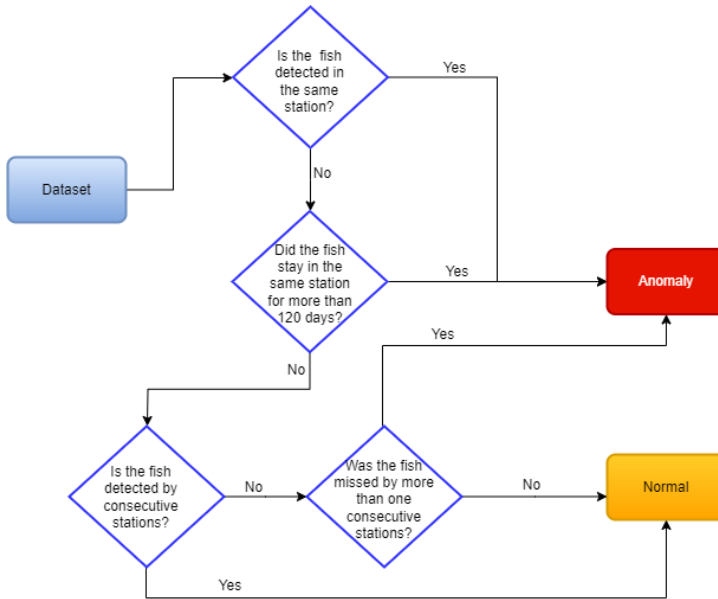


Figure 4 Flowchart for anomaly detection in the acoustic telemetry test dataset comprising 50 dusky kob tagged and monitored in the Breede Estuary between 2016 and 2021.

Any detection meeting at least one of the defined criteria mentioned above was marked as an anomaly (label 0), while the rest were considered normal (label 1). To ensure data quality and a robust foundation for an anomaly detection system, the labelled data underwent validation, and detected anomalies were manually reviewed by a domain expert to confirm their validity. The complete flowchart of labelling is visually depicted in Figure 4.

The initial dataset contained 3038671 detections. During data pre-processing, duplicates were removed, resulting in 3013930 unique detections. After labelling, 2754230 detections (91.38%) were identified as “normal”, while 259700 (8.62%) were classified as “anomalies”. The significant imbalance of 91.38% normal detections to 8.62% anomalies led us to choose unsupervised learning classifiers, which do not require balanced datasets, unlike supervised classifiers. The unsupervised classifiers were trained to recognize only normal patterns. When tested with both normal and anomalous patterns, they failed to recognize the anomalies, allowing us to flag such detections. Although unsupervised classifiers typically require less manual data preparation, in this study, we labelled the data to specifically train the models on normal patterns and then used the anomalous patterns to interpret the classifiers outcomes.

2.6 Resampling acoustic telemetry data from real data

The sampling rate is determined by the frequency of normal and anomalous detections at specific times. In this study, the acoustic telemetry data were sampled irregularly on a daily basis and varied each day over the observation period. Figure 5 illustrates the detection of the same fish over three days. The horizontal axis represents the time of day when the fish was detected, clearly indicating that detections do not occur at regular intervals, which was expected in an acoustic telemetry dataset due to fish varying their movements on a daily basis linked to environmental variables (e.g. temperature, salinity, turbidity, river flow, etc.) and cyclical rhythms (i.e. movements influenced by time of day, tidal cycle, moon phase, etc.). This irregularity can impact the accuracy of the classifiers being trained. Since we are training unsupervised classifiers only on the normal patterns, we employ a resampling strategy that adjusts the irregular sampling of the normal samples. This strategy aims to approximate the Nyquist sampling requirements, not necessarily to balance the data. A consistent sampling rate was vital for preserving the signal's integrity, crucial for precision analysis. Well-sampled data allows models to learn more effectively, providing a reliable representation of the underlying signal, which in turn facilitates feature extraction and enhances model performance.

Our strategy actively adjusted the sampling rate to reflect daily changes in data collection. This adjustment was based on calculating the minimum of the shortest non-zero time intervals between consecutive data points, labelled as $\Delta^d t$, where the subscripts d indicated that this varied per day:

$$\Delta^d t = \min(\{t_{i+1} - t_i\}), \quad i = 1, \dots, N_t \quad (2)$$

where t_i and t_{i+1} represent the consecutive timestamps of data points during day d and N_t was the number of normal detection timestamps. To standardize the sampling rate across all days, we chose the minimum $\Delta^d t$ across days:

$$\Delta t = \min(\{\Delta^d t\}), \quad d = 1, \dots, N \quad (3)$$

where N was the total number of monitored days. The sampling rate was then the inverse of Δt given as:

$$f_s = \frac{1}{\Delta t}. \quad (4)$$

This sampling rate sets the frequency at which data points were collected, helping to generate new data points at approximately consistent intervals.

After implementing the resampling strategy described in Equation 4, we observed a pattern that approximated regular sampling. However, this was accompanied by computational challenges due to the high resampling rate,

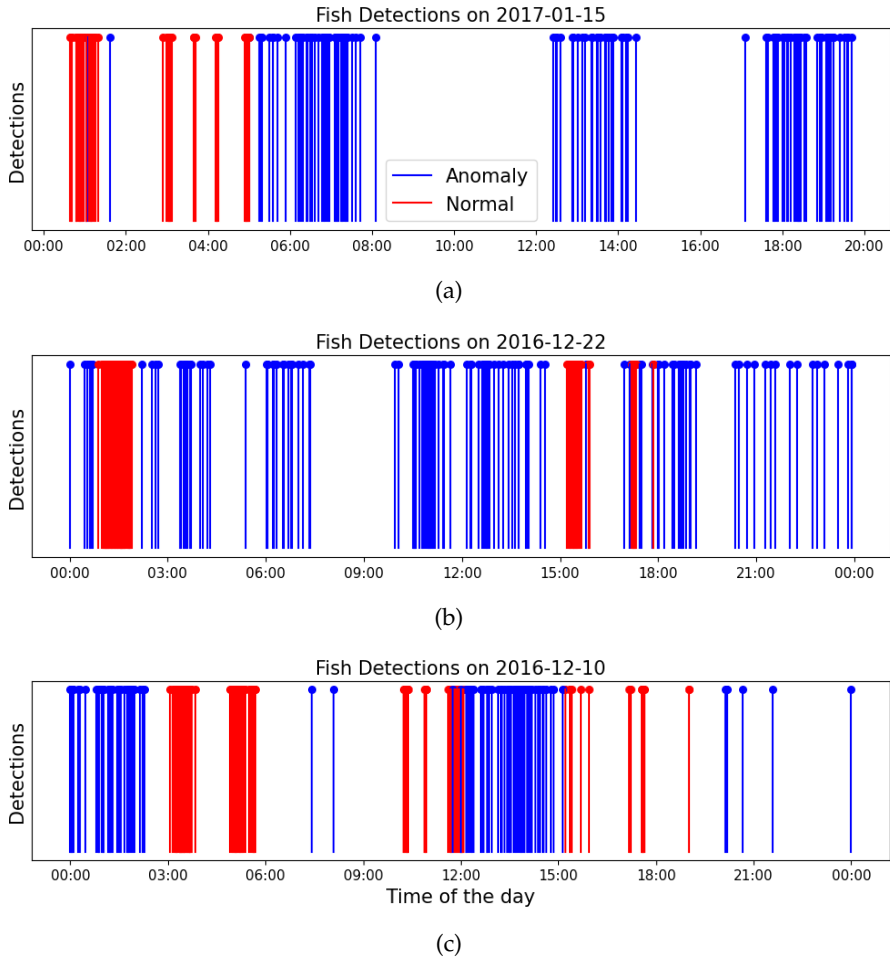
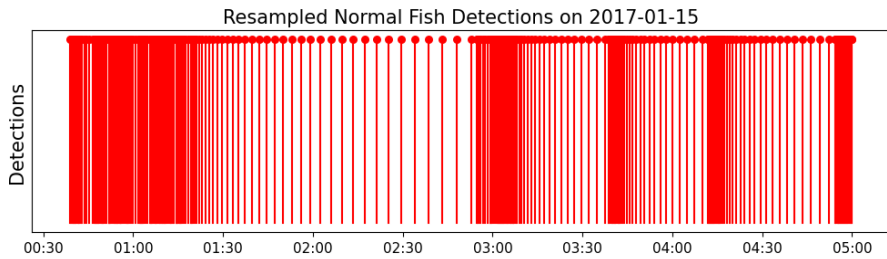
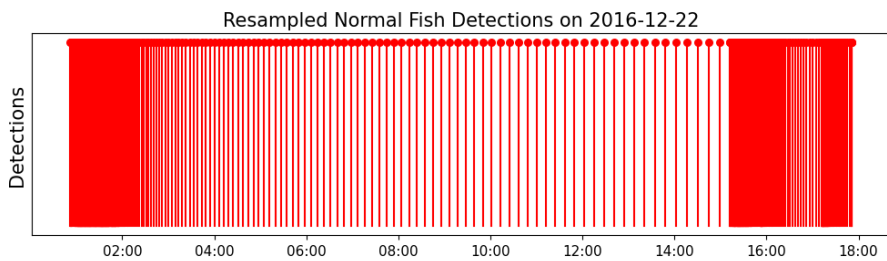


Figure 5 Examples of fish detections across three different days 2017-01-15 (a), (2016-12-22 (b) and 2016-12-10(c)) show irregular sampling patterns in acoustic telemetry data. The horizontal axis represents the time of day, while the vertical markers differentiate between normal (red) and anomalous (blue) detections. The varying frequency and irregular intervals of detections show the challenges of missing data and the importance of resampling strategies to preserve signal integrity and improve unsupervised classifier performance.

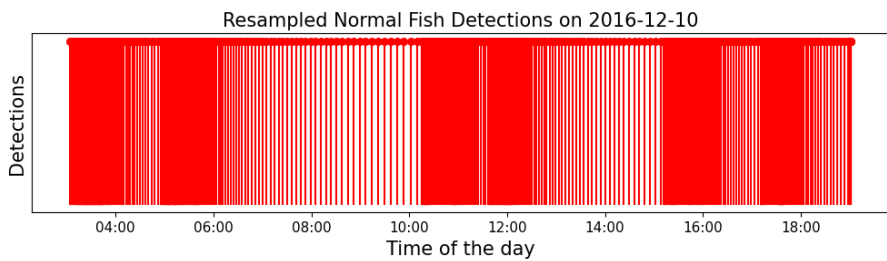
which necessitated significant computational resources to train the classifiers. Instead of using the minimum rate as specified in Equation 4, we iteratively resampled using the next smallest rate until we found a trade-off between sampling regularity and computational feasibility for training the classifiers. With the adjustment following the trade-off search, the data in Figure 5 now exhibit an approximate regularity as shown in Figure 6.



(a)



(b)



(c)

Figure 6 Comparison of resampled normal fish detections across three different days: 2017-01-15 (a), 2016-12-22 (b) and 2016-12-10 (c). Each day is resampled with the smallest sampling rate among the three days, approximating regular intervals. The resampling strategy is designed to adjust for irregular sampling patterns and ultimately improve the performance of unsupervised classifiers.

2.7 Unsupervised classifiers

We trained three widely used traditional unsupervised classifiers for anomaly detection: IF, LOF, and DBSCAN. Additionally, we trained a NN-AE and a long short-term memory-based autoencoder (LSTM-AE). IF employs tree structures and random partitioning to detect outliers in complex datasets. By randomly selecting features and partitioning the data to isolate observations, IF constructs isolation trees and calculates an anomaly score

based on the path length from the root node to each data point — shorter paths indicate potential anomalies [35, 36]. LOF assesses the local density deviation of a data point relative to its neighbours, focusing on localized density rather than a global density metric. By comparing a point’s density to its surrounding neighbourhood, LOF assigns an outlier score that highlights points that deviate locally, which makes it particularly suited for detecting outliers in dense data regions [37–39]. DBSCAN is used as a density-based clustering algorithm that groups points according to density and labels any points not associated with clusters as noise or outliers. DBSCAN identifies dense regions by core points and forms clusters based on reachability; any points unreachable by core points are classified as noise, making DBSCAN highly effective for data with varied cluster shapes and densities [40–42].

Neural networks are computational models inspired by the human brain, consisting of layers of interconnected nodes (neurons) that process and learn from data [43]. An autoencoder consists of an encoder, a latent space, and a decoder. The encoder compresses the input into a latent-space representation, and the decoder reconstructs the input data from this representation assuming a reconstruction error [44, 44–46]. The reconstruction error, or the difference between the original and reconstructed data, serves as the primary indicator of anomalies [45]. One of the challenging tasks for AEs is determining the optimal threshold to bound the reconstruction errors. In this paper, we introduced an additional block that finds this optimal threshold for the reconstruction error, and any data point exceeding this threshold was considered anomalous.

Although the traditional models allow quick training without extensive hyperparameter tuning, they were prone to high false normal rates (that is, they predicted anomalous as normal). This limitation arose because certain legitimate anomalies shared features with normal data points, making them difficult for traditional models to distinguish, leading to misclassifications. However, traditional models demonstrated competitive performance compared to NN-AE in minimizing false anomalies (i.e., predicting normal instances as anomalous). The LSTM-AE quickly overfitted the data, even after resampling efforts. Due to the limitations observed with the LSTM-AE model, this paper focuses exclusively on the performance of traditional models and NN-AE as baseline models for the detection of telemetry anomalies.

2.8 Performance metrics

We evaluated the models using several performance metrics, including the confusion matrix, Receiver Operating Characteristic (ROC) curve, accuracy, precision, recall, specificity, and F_1 -score. The confusion matrix summarizes the model’s predictions into four categories: True anomalies (TA) refer to the number of anomalous samples that are correctly identified as anomalous. False anomalies (FA) are the number of normal samples incorrectly classified

Table 3 Summary of key classification metrics used to evaluate model performance. Each metric provides distinct insights into the model’s ability to correctly classify normal and anomalous instances.

Name	Description	Formula
accuracy	The proportion of correctly classified instances among the total instances.	$\frac{TA+TN}{TA+TN+FA+FN}$
precision	The ratio of true anomaly predictions to the total number of positive predictions, indicating how often the model is correct when it predicts a positive outcome.	$\frac{TA}{TA+FA}$
recall	The ratio of true anomalies to the total actual anomalies, measuring the model’s ability to identify positive instances.	$\frac{TA}{TA+FN}$
specificity	The ratio of true normals to the total actual negatives, indicating how well the model identifies negative instances.	$\frac{TN}{TN+FA}$
F ₁ -score	The harmonic mean of precision and recall. It balances the two metrics, especially in cases of imbalanced class distributions.	$\frac{2 \times \text{precision} \times \text{recall}}{\text{precision} + \text{recall}}$

as anomalous. True normals (TN) represent the number of normal samples that are correctly classified as normal, while false normals (FN) are the number of anomalous samples that are incorrectly classified as normal. These values are the basis for calculating the other metrics in Table 3. The ROC curve is a graphical representation of a model’s ability to distinguish between classes. It plots the true anomaly rate against the false anomaly rate at various threshold settings. The area under the ROC curve (AUC) indicates the model’s overall performance, with a value of 1 representing a perfect model.

2.9 Experimental design

Figure 7 provides a comprehensive overview of the experimental design, encompassing each stage from data pre-processing and dataset splitting to resampling, training, hyperparameter tuning, and testing.

In *Step 1*, the data underwent pre-processing, which included handling missing values, removing duplicates, and performing feature engineering. After pre-processing, the data moved to *Step 2* for various splits. Initially, the dataset was divided into two main categories: normal and anomalous samples. Normal samples accounted for 91.2% of the data (2749960 samples), while anomalous samples made up 8.8% (263970 samples) of the original dataset.

For the normal samples, 10% (274996 samples) was set aside for testing, and the remaining 90% (2474964 samples) underwent resampling as described in Section 2.6. The resampled data was then used to train the traditional models without any further splitting. For the NN-AE model, the resampled data was further divided into 80% for training and 20% for validation. Note that the 10% test data was not resampled.

For the anomalous samples, 50% (131985 samples) was allocated for testing, while the other 50% (131985 samples) was used for training the traditional models and also served for validation to determine the autoencoder threshold, as discussed in Section 2.7. The splitting strategy outlined indicated that the traditional models were trained using both normal and anomalous data, while the NN-AE model was trained exclusively on normal data.

After *Step 2*, the data proceeded to *Step 3* for training and hyperparameter tuning. For each model, hyperparameter tuning was performed using the GridSearch algorithm [47]. The IF model optimally detected anomalies by recursively partitioning data points with 100 estimators and a contamination setting of 0.001, balancing robustness and computational efficiency. The LOF identified anomalies by evaluating the local density deviation of each point relative to its neighbours, using 5 neighbours and a contamination parameter of 0.01. For DBSCAN, the optimal parameters were determined to be an epsilon value of 0.5 and a minimum sample size of 10. For the NN-AE, hyperparameter tuning was conducted using the validation set, which contained both normal and anomalous samples, in order to determine the optimal threshold for the autoencoder. The optimal configuration for the NN-AE consisted of a learning rate of 0.001, 128 units per layer, and 2 units in the compression layer. The model was trained with a batch size of 512 over 50 epochs. Table 4 summarized the range of hyperparameters and their optimal values determined via GridSearch.

After training and hyperparameter tuning, the models proceeded to *Step 4* for testing. The test data, set aside during the splitting step (prior to resampling and training), contained both normal and anomalous instances and was used to evaluate the models' ability to accurately detect anomalies.

3 Results and discussion

The results of the models, trained with the optimal hyperparameters as discussed in Section 2.9, were analysed, compared, and interpreted, and are discussed in this section.

3.1 Finding optimal threshold

Among the metrics of precision, recall, and specificity we aim to maximize the recall, as this indicates that the model has maximized the detection of true anomalies while minimizing the prediction of anomalies as normal instances (i.e., minimizing FN). This is crucial for telemetry observations, as the presence of FN in the data might skew the scientific interpretation for which the telemetry data were observed. The goal is to achieve a recall of 1, which ensures that no FN are present in the observations. For the range of thresholds where recall is maximized, we then select the threshold that also maximizes both precision and specificity to reduce the identification of false anomalies (i.e. minimizing FA).

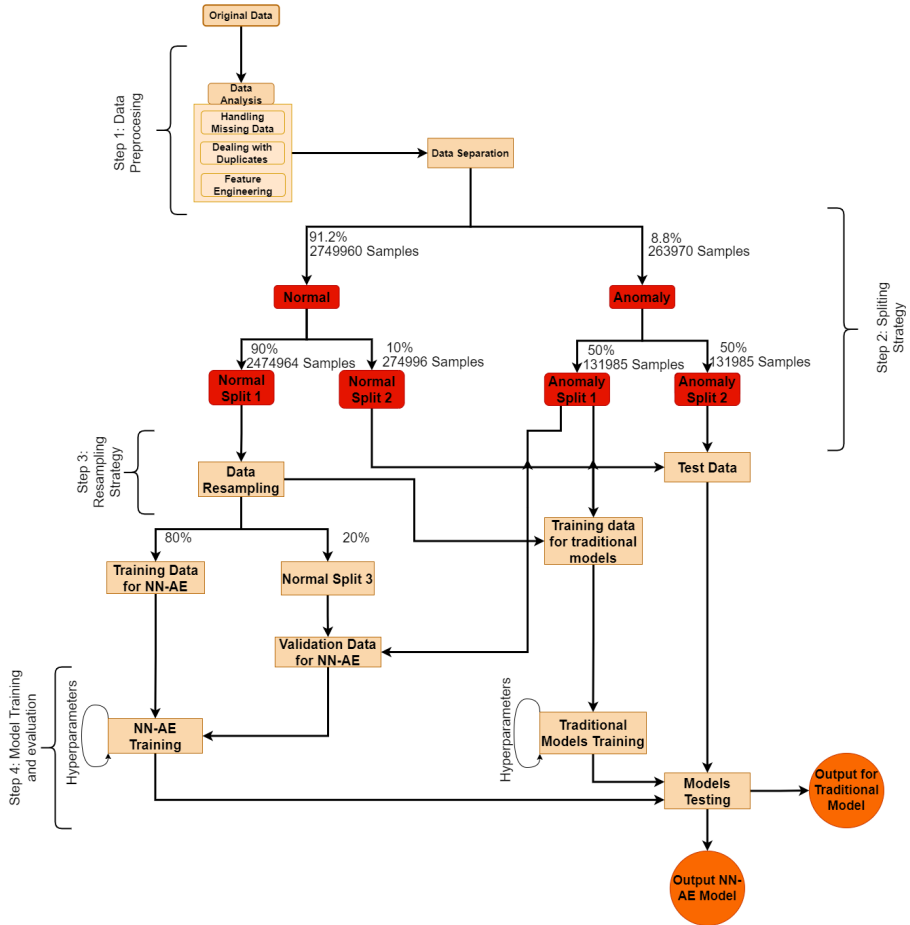


Figure 7 The diagram shows an anomaly detection workflow with data pre-processing, followed by data splitting into training and testing sets, and concludes with model training and testing for both the NN-AE and traditional models used in this work.

The algorithm works as follows. Assume that the percentiles run from $i = 1, \dots, n$ where each percentile corresponds to a specific threshold. Let $R = \{r_i\}$ be the recall set where each r_i is the recall for percentile i , $P = \{p_j\}$ be the precision set where j corresponds to selected indices from R , and $S = \{s_k\}$ be the specificity set where k corresponds to selected indices from P . The algorithm consists of three steps: the first step finds the maximum values in R ; $R_{\max} = \max\{r_i : i = 1, \dots, n\}$ and identify all indices j where $R_j = R_{\max}$, i.e. the indices of the maximum values in R ; $J = \{j : R_j = R_{\max}\}$. The second step finds the maximum value in P for $j \in J$; $P_{\max} = \max\{p_j : j \in J\}$ and identifies all indices k where $P_k = P_{\max}$, i.e. the indices of the maximum values in P ; $K = \{k : P_k = P_{\max} \text{ and } k \in J\}$. The final step finds the maximum value in S for $k \in K$; $S_{\max} = \max\{s_k : k \in K\}$ and produces all the indices l where $S_l = S_{\max}$. The best percentile is any of the l percentiles.

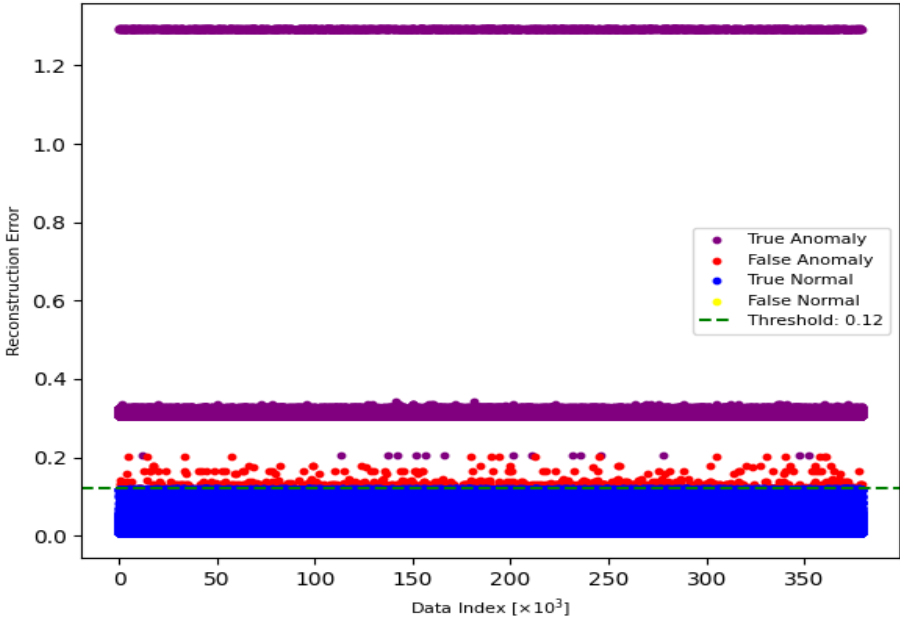


Figure 8 Reconstruction errors plotted against the data index, highlighting TN (blue), TA (purple), FA (red), and FN (yellow) using the validation datasets without resampling. Higher reconstruction errors indicate potential anomalies.

As shown in Tables A1, A1, and A2, the optimal percentiles identified by the algorithm are the 65th, 67th, and 69th percentiles for the datasets without resampling, with 90s resampling, and with 65s resampling, respectively. Figure 8 shows the corresponding threshold for 65th percentile, where the reconstruction errors are plotted against the indices of the validation dataset without resampling.

3.2 Performance

Using the optimal parameters, the confusion matrix generated from the classifiers' predictions on the test set is shown in Figure 9, with the top panel depicting models trained on data without resampling, and middle and bottom panels showing models trained on resampled data at 90s and 65s, respectively. Figure 10 provides a detailed visualization of TA, FA, TN, and FN derived from the confusion matrix of the data without resampling, with 90s resampling, and with 65s resampling. These results offer a comprehensive overview of the models' performance, warranting a thorough discussion to evaluate their strengths and weaknesses in classifying normal and anomalous detections.

The results revealed that IF outperformed other models by eliminating FA, with NN-AE minimizing FA compared to LOF and DBSCAN. Resampling at finer rates decreased FA for NN-AE but not for other models, reflecting NN-AE's enhanced performance through increased data size and high-resolution data. This improvement stems from the model's ability to capture subtle patterns, reduce overfitting, and generalize more effectively with increased data size, unlike LOF and DBSCAN, which reach performance saturation quickly where additional data no longer yields significant improvement [48]. In telemetry studies, these findings are noteworthy. As telemetry datasets grow continuously with each new recording, a model capable of handling large datasets is essential, and minimizing FA is important. Detecting a high rate of FA would mean that a substantial portion of normal data is misclassified as anomalous, and therefore removed from the telemetry observation. The removal of a substantial portion of normal data could skew the primary analyses for which the telemetry data are collected for.

The results indicate that NN-AE achieves a 100% TA detection rate (i.e. no FN), which is crucial for telemetry observations, as it ensures that all anomalies are eliminated, leaving only normal samples. However, a very small fraction of FA; i.e. ~ 0.00352 of normal samples was also misclassified as anomalies and subsequently removed. This minimal removal of normal samples had no significant impact on data quality, as telemetry observations operate at a big data scale, making the loss of such a small fraction of data negligible.

Figures 11 and C2 present the performance metrics of the models, including accuracy, F_1 -score, recall, precision, specificity, and AUC, with error bars indicating the confidence intervals for each metric. A narrow confidence interval suggests a stable estimate, meaning repeated data reshuffling and splitting would yield similar results. In contrast, a wider confidence interval implies an unstable estimate, reducing its reliability. The results clearly demonstrate that NN-AE outperformed the other models with only specificity from other models competing comparably. This was attributed to all models showing a capability to minimize the FA, as discussed in Section 3.1. The values used to generate Figure 11 are detailed in Table C4, which provides a comprehensive breakdown of each metric and includes information on the computational requirements and confidence intervals of each model.

Training times generally increase under resampling conditions. For the IF model, training times range between 4.17 minutes and 4.74 minutes. For LOF models, training times range from 24.61 minutes to 32.48 minutes. The DBSCAN model requires training times between 8.92 minutes and 9.44 minutes. All NN-AEs require significant training time, ranging from 11.6 hours to 14.2 hours. While these computation times may seem high during training, NN-AEs are generally fast when deployed. All experiments were conducted on a system with a 12th Gen Intel[®] Core[™] i7-12700 CPU @ 2.10 GHz, 16 GB

Table 4 This table presents optimal hyperparameters selected for each anomaly detection model used in the work: IF, LOF, DBSCAN, and NN-AE. The models were tuned using various hyperparameter options, as listed in the "Hyperparameter" column. The "Best Parameter" columns show the selected hyperparameter values under three conditions: no resampling, resampling at 90s, and resampling at 65s.

Model	Hyperparameter	Best Parameter		
		No	90s	65s
IF	Contamination: [0.001, 0.02, 0.05, 0.3]	0.001	0.001	0.001
	Number of Estimators: [100, 150, 200]	100	100	100
LOF	Number of Neighbors: [5, 10, 20]	5	5	5
	Contamination: [0.01, 0.08, 0.1, 0.2]]	0.01	0.01	0.01
DBSCAN	Epsilon: [0.5, 1.5, 2, 3.5, 5]	0.5	0.5	0.5
	Minimum Samples: [2, 4, 10]	10	10	10
NN-AE	Learning Rate: [0.001, 0.01, 0.1]	0.001	0.001	0.001
	Units Layer: [4, 8, 16, 32, 64, 128]	128	128	128
	Compression Layer Units: [2, 4, 8]	2	2	2
	Batch Size: [128, 256, 512]	512	512	512
	Epochs: [20, 50]	50	50	50

RAM, running Windows 11 Enterprise (Version 23H2) with Python 3.12.7, TensorFlow 2.18.0, and scikit-learn 1.5.1.

3.3 Interpretability of the NN-AE detection of FA and FN

Understanding the mechanisms behind NN-AE models' predictions of FA and FN provides valuable insights into the nature of anomalies and their correlations with normal data. Such an analysis can reveal patterns in telemetry datasets, helping to distinguish between true anomalies and noise or artifacts in the data. This is particularly relevant for the study of telemetry, where the boundary between normal and anomalous behaviour can be complex and context-dependent. There were three types of anomalies in the dataset: (i) fish recorded at only one station, (ii) normal/expected movements, but then remained stationary for more than 120 days, and (iii) a fish passing more than one consecutively positioned receiver.

The NN-AE model showed strong performance in detecting anomalies in which fish were recorded at a single station throughout the study period, flagging all instances of this type of anomaly.

The second anomalous behaviour was not present in our dataset, preventing the NN-AE model from being tested on this criterion. To prepare the model for future scenarios where such behaviour might occur, synthetic data simulating such prolonged stays or expanding the dataset to capture more rare events would be beneficial. This would enhance the model's ability to detect and learn from extreme cases, improving its overall reliability in detecting anomalies.

Resampling		IF	DBSCAN	LOF	NN-AE				
Without resampling	Actual Normal	274996	0	268314	6682	271462	3534	274031	969
	Actual Anomaly	131843	142	131656	329	131449	536	0	131985
Resampling 90s	Actual Normal	274996	0	268314	6682	271462	3534	274077	919
	Actual Anomaly	131784	201	131656	329	131449	536	0	131985
Resampling 65s	Actual Normal	274996	0	268314	6682	271462	3534	274394	602
	Actual Anomaly	131764	221	131656	329	131449	536	0	131985
		Normal	Anomaly	Normal	Anomaly	Normal	Anomaly	Normal	Anomaly
		Predicted		Predicted		Predicted		Predicted	

Figure 9 Confusion matrices for different anomaly detection models (NN-AE, DBSCAN, IF, LOF) applied to telemetry data, comparing "Normal" and "Anomaly" classifications at different sampling rates (65s and 90s).

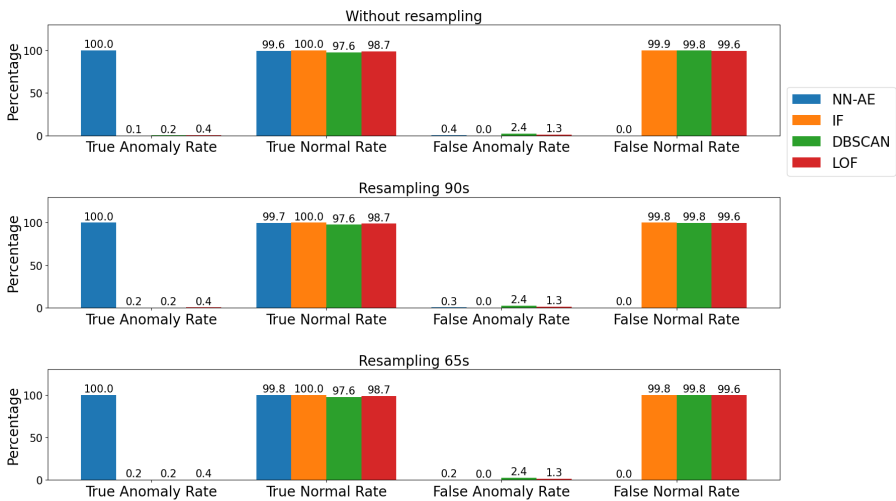


Figure 10 This bar chart shows the key metrics of the confusion matrix TA, TN, FA, and FN for anomaly detection models (NN-AE, IF, DBSCAN, LOF). The performance is compared across three conditions: without resampling, with 90s resampling, and with 65s resampling. NN-AE achieves the highest TA and TN rates, indicating its strong performance in anomaly detection. IF has a higher false normal rate, while DBSCAN and LOF have balanced but slightly lower detection capabilities.

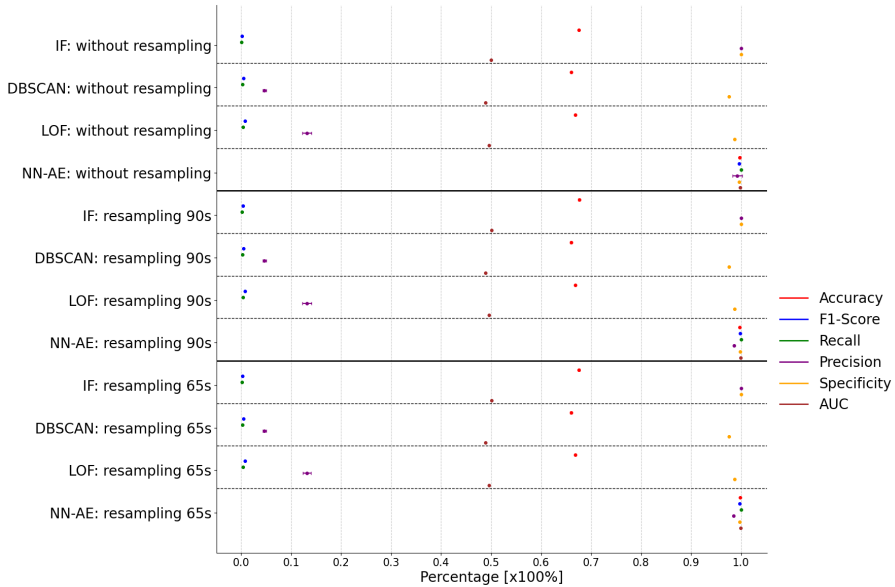


Figure 11 This figure compares the performance of different anomaly detection models (LOF, DBSCAN, IF, and NN-AE) across six metrics: accuracy, F_1 -score, recall, precision, specificity, and AUC, along with confidence intervals. Model variations (e.g., LOF_65s, DBSCAN_90s) show differing levels of performance on these metrics across varying sampling rates. NN-AE performs consistently well in AUC and accuracy, while the other models exhibit more variation in precision and recall.

The model effectively identified anomalies where fish were missed by more than one consecutive station. It flagged all true anomalies without any false normals, but some normal movement patterns with occasional detection gaps were incorrectly classified as anomalies (see Appendix B for a detailed discussion).

The models also misclassified as anomalies some normal detections that did not align with any of the three expert-defined criteria (see Appendix B for a detailed discussion), suggesting they occasionally flag unusual but not truly anomalous patterns. This over-sensitivity to movement pattern variations highlights a key challenge in automated anomaly detection for fish telemetry data: distinguishing between genuinely anomalous behaviour and natural behavioural variability. This limitation underscores the importance of incorporating biological knowledge and expert validation in the development and refinement of machine learning models for ecological applications. Future work could focus on training models with more diverse examples of normal movement patterns or implementing additional context-aware features that better account for natural behavioural variability.

3.4 Discussion

NN-AE demonstrated an exceptional performance by showing no FN, a critical factor in ensuring that no true anomalies were missed. In contrast, IF, DBSCAN, and LOF exhibited significantly higher FN fractions of ~ 0.9989 , ~ 0.9975 , and ~ 0.9959 , respectively, on the dataset without resampling. These high FN fractions indicated that these models failed to detect nearly all true anomalies, which is a considerable limitation, particularly in applications like telemetry observations where missing anomalies can impact the interpretation of movement patterns. Moreover, these models did not show any meaningful improvement in reducing FN rates when resampling techniques were applied. This lack of responsiveness to resampling highlights their limited adaptability to variations in the data distribution and reinforces their unsuitability for high-stakes anomaly detection tasks where the identification of true anomalies is paramount. The absence of FN in NN-AE underscores its robustness and reliability in anomaly detection tasks, making it a superior choice for datasets where accuracy in identifying anomalies is essential. This advantage is particularly pronounced in dynamic and large-scale datasets, such as those encountered in telemetry studies, where ensuring the complete identification of anomalies is critical for maintaining the integrity of the analysis.

In terms of FA, IF showed no FA detections, while NN-AE reports a negligible FA fraction of ~ 0.00352 . This minimal FA rate in NN-AE further decreased when resampling techniques were applied, demonstrating its adaptability and capacity to improve its performance with data resampling. On the other hand, DBSCAN and LOF exhibited FA fractions of approximately ~ 0.0242 and ~ 0.0128 , respectively, on the dataset without resampling. Unlike NN-AE, these models showed no reduction in FA rates even with the application of resampling techniques, highlighting their limited ability to adapt to data resampling.

The differences in FN and FA rates among these models underscore their varying capabilities and limitations in anomaly detection tasks. NN-AE's superior performance, marked by the absence of FN detections and negligible FA rates that further reduce with resampling, makes it particularly suitable for critical applications like telemetry, where both the identification of TA and the minimization of FA are essential.

While this work demonstrates the impressive capabilities of the NN-AE model in accurately detecting anomalies, it also brings to light certain limitations that warrant further discussion. One significant challenge was the computational demand associated with training and optimizing the NN-AE model. Given the complexity of the architecture and the volume of data often encountered in telemetry and other large-scale applications, the model required substantial computational resources, which can be a limiting factor

in environments with constrained infrastructure or limited access to high-performance computing. Another noteworthy limitation was the occurrence of false anomaly detections, where normal behaviour was misclassified as anomalous. Although the FA fraction ~ 0.00352 observed in this study was exceptionally low, such misclassifications, however negligible, may still have implications depending on the application. For instance, in critical domains like telemetry, monitoring even minimal false anomalies could lead to unnecessary interventions in the field. Nonetheless, it is worth emphasizing that the FA rate of the NN-AE model was significantly negligible compared to alternative models like DBSCAN or LOF, which exhibit much higher FA rates and failed to improve with resampling. The balance between computational efficiency and detection accuracy poses an ongoing trade-off in anomaly detection frameworks. While the NN-AE model offers a clear advantage in terms of recall, precision, and adaptability, its computational intensity highlights the need for future research into more resource-efficient algorithms that retain comparable performance. Additionally, incorporating deep learning explainability mechanisms into the NN-AE model could enhance its applicability by providing insights into the specific features or patterns leading to false anomaly detections. This could help refine the model further and reduce even the negligible rates of misclassification.

4 Conclusion

This study focused on dusky kob acoustically tagged in the Breede Estuary, providing valuable insights into anomaly detection in fish movement patterns using acoustic telemetry data. While the findings are robust, their specificity may limit their generalizability to other species, estuaries, or regions. Variations in environmental conditions, such as water temperature, salinity, or habitat structure, necessitate recalibrating or retraining models when applied to new ecosystems. Furthermore, movement patterns, habitat preferences, and/or behaviours are often species-specific, and as such, each dataset may exhibit anomalies differently, requiring tailored feature engineering and anomaly detection techniques to maintain accuracy.

The results clearly demonstrate the effectiveness of the NN-AE model in anomaly detection. With accuracy, precision, and recall significantly outperforming traditional unsupervised learning models such as IF, LOF, and DBSCAN across all evaluation metrics, except for specificity, where IF achieved the highest performance, followed closely by the NN-AE model. These results underscore the NN-AE model's ability to capture complex temporal dependencies in time series data, enabling the detection of subtle anomalies that traditional methods often overlook. Such capabilities are critical for telemetry studies and conservation efforts, where understanding anomalies in fish behaviour is essential for assessing ecosystem dynamics, habitat usage, and responses to environmental changes.

The practical implications of this work are substantial. By automating anomaly detection, the NN-AE model reduces the need for labour-intensive manual data review, enabling researchers to focus on higher-level ecological analyses and conservation strategy development. In fisheries management, early detection of behavioural anomalies could alert stakeholders to threats such as habitat degradation, poaching, or disease outbreaks, facilitating timely interventions.

However, this study also highlights areas for improvement and future exploration. Expanding the dataset to include a broader range of species and environmental conditions is critical to improving the generalizability and robustness of the model. Enhancing the model's ability to detect slow deviations from expected movement patterns remains a priority. Exploring adaptive thresholds that dynamically adjust based on temporal data patterns could refine detection capabilities, particularly for subtle, gradual anomalies. Furthermore, integrating attention-based approaches could further enhance its capacity to minimise false anomalies.

In conclusion, this study demonstrated the transformative potential of machine learning, particularly NN-AE models, in automating anomaly detection in acoustic telemetry data. Beyond technical success, the ecological significance of this work is profound. Detecting movement anomalies provides crucial insights into environmental changes, human impacts, and fish health. This information is instrumental in developing conservation measures, such as identifying signs of habitat destruction, illegal fishing activities, or climate change effects on aquatic ecosystems. While the findings are directly applicable to dusky kob in the Breede Estuary, the methodology provides a scalable framework for studying other species and environments, contributing to global conservation efforts and advancing the role of artificial intelligence in ecological research.

CRedit authorship contribution statement

Siphendulwe Zaza: Conceptualization, Data curation, Formal analysis, Investigation, Methodology, Software, Visualisation, Writing – original draft, Writing – review & editing. **Marcellin Atemkeng:** Conceptualization, Methodology, Visualisation, Formal analysis, Resources, Writing – review & editing, Supervision, Validation. **Taryn S. Murray:** Conceptualization, Formal analysis, Visualisation, Data curation, Resources, Fieldwork, Writing – review & editing, Supervision, Validation. **John David Filmlalter:** Data curation, Fieldwork, Resources, Writing – review & editing, Validation. **Paul D. Cowley:** Funding acquisition, Resources, Validation.

Data availability

Data will be made available on request.

Acknowledgments

The Acoustic Tracking Array Platform (ATAP) is hosted by the South African Institute for Aquatic Biodiversity, a National Facility of the National Research Foundation (NRF-SAIAB). The Ocean Tracking Network (OTN) headquartered at Dalhousie University, Canada, the Department of Science and Innovation-Shallow Marine and Coastal Research Infrastructure program, and the South African Environmental Observation Network Elwandle Node (NRF-SAEON Elwandle Node) are thanked for providing acoustic telemetry hardware that facilitated data collection for this study. Furthermore, the Save Our Seas Foundation and the African Coelacanth Ecosystem Programme are acknowledged for funding to maintain the national ATAP. Dr JD Filmlter is thanked for his efforts in tagging all fish for this study, as well as maintaining the acoustic receiver array positioned in the Breede Estuary. Further, funding for acoustic transmitters and project running expenses were funded by the South Africa–Norway Cooperation on Ocean Research (SANOCEAN Project No. 287015). Siphendulwe Zaza thanks LEVENSTEIN, THE ADA & BERTIE for the financial support. Marcellin Atemkeng thanks the National Research Foundation of South Africa for support through project number CSRP23040990793.

Appendix A

Tables [A1](#), [A2](#), and [A3](#) show the optimal thresholds for NN-AE trained and validated on three datasets: the original dataset without resampling, with 90s resampling, and with 65s resampling, respectively. The optimal percentile thresholds were 65 for the model trained on the dataset without resampling, 67 for the 90s resampling dataset, and 69 for the 65s resampling dataset. This trend suggests that datasets with higher temporal resolution (i.e., shorter resampling intervals) required slightly higher percentile thresholds for optimal anomaly detection.

Appendix B

We categorized all false anomalies identified by models trained and validated on the three datasets. The categorization process involved identifying false anomalies that resemble each of the three predefined anomaly criteria.

Figure [B1](#) shows the distribution of false anomalies for the datasets without resampling (a), with 90s resampling (b), and with 65s resampling (c), respectively. Red indicates false anomalies that do not resemble any predefined anomaly criteria (classified as unknown). Yellow are the false anomalies that resemble anomaly type *fish recorded at only one station* (Criterion 1), green are false anomalies that resemble anomaly of type *normal/expected movements, but then remained stationary for more than 120 days* (Criterion 2), and blue are false anomalies that resemble anomaly type *a fish passing more than one consecutively*

Table A1 Performance metrics at different percentiles of reconstruction errors, demonstrating the trade-offs, and supporting the selection of the 65th percentile as the optimal threshold for anomaly detection in data without resampling.

Percentile	Optimal Threshold	precision	recall	F ₁ -score	specificity	accuracy
1	0.007764	0.351275	1.0	0.519917	0.015156	0.357688
2	0.008336	0.354852	1.0	0.523824	0.030457	0.367667
3	0.008481	0.358488	1.0	0.527775	0.045702	0.377609
4	0.009629	0.362266	1.0	0.531858	0.061213	0.387726
5	0.009824	0.366179	1.0	0.536064	0.076946	0.397987
6	0.010049	0.370074	1.0	0.540225	0.092272	0.407982
7	0.011195	0.374071	1.0	0.544471	0.107670	0.418025
8	0.011339	0.378028	1.0	0.548650	0.122591	0.427757
9	0.011383	0.382179	1.0	0.553009	0.137913	0.437749
10	0.011512	0.386402	1.0	0.557417	0.153165	0.447697
11	0.011848	0.390943	1.0	0.562126	0.169194	0.458151
12	0.012492	0.395418	1.0	0.566738	0.184633	0.468220
13	0.012549	0.399941	1.0	0.571369	0.199885	0.478168
14	0.012802	0.404536	1.0	0.576042	0.215029	0.488044
15	0.013133	0.409309	1.0	0.580865	0.230403	0.498071
16	0.014166	0.414214	1.0	0.585786	0.245829	0.508132
17	0.014493	0.419164	1.0	0.590719	0.261033	0.518048
18	0.014778	0.424363	1.0	0.595864	0.276622	0.528215
19	0.015240	0.429626	1.0	0.601033	0.292016	0.538255
20	0.015895	0.435106	1.0	0.606375	0.307648	0.548450
21	0.016621	0.440711	1.0	0.611796	0.323236	0.558617
22	0.017105	0.446431	1.0	0.617286	0.338739	0.568728
23	0.018964	0.452512	1.0	0.623075	0.354792	0.579197
24	0.019656	0.458394	1.0	0.628629	0.369916	0.589061
25	0.020551	0.464440	1.0	0.634290	0.385059	0.598937
26	0.021317	0.470800	1.0	0.640196	0.400571	0.609054
27	0.021895	0.477062	1.0	0.645961	0.415439	0.618751
28	0.022122	0.483591	1.0	0.651919	0.430530	0.628594
29	0.023237	0.490313	1.0	0.658000	0.445650	0.638455
30	0.023745	0.497471	1.0	0.664415	0.461299	0.648661
31	0.024585	0.504572	1.0	0.670719	0.476386	0.658500
32	0.025161	0.511943	1.0	0.677199	0.491602	0.668424
33	0.025700	0.519722	1.0	0.683970	0.507194	0.678593
34	0.027399	0.527657	1.0	0.690806	0.522625	0.688657
35	0.029553	0.535921	1.0	0.697850	0.538209	0.698821
36	0.029990	0.544445	1.0	0.705037	0.553789	0.708982
37	0.030776	0.553183	1.0	0.712322	0.569259	0.719072
38	0.031713	0.562112	1.0	0.719682	0.584573	0.729060
39	0.032265	0.571391	1.0	0.727242	0.599979	0.739108
40	0.033151	0.581078	1.0	0.735041	0.615539	0.749256
41	0.034136	0.590770	1.0	0.742747	0.630594	0.759074
42	0.035481	0.600762	1.0	0.750595	0.645608	0.768867
43	0.037271	0.611319	1.0	0.758781	0.660937	0.778864
44	0.038495	0.622107	1.0	0.767036	0.676065	0.788730
45	0.038779	0.633444	1.0	0.775593	0.691406	0.798736
46	0.039302	0.644767	1.0	0.784022	0.706190	0.808378
47	0.041025	0.656769	1.0	0.792831	0.721306	0.818236
48	0.041799	0.669638	1.0	0.802136	0.736910	0.828413
49	0.043906	0.682682	1.0	0.811421	0.752126	0.838338
50	0.044223	0.696193	1.0	0.820889	0.767286	0.848225

Table A1 Cont.

Percentile	Optimal Threshold	precision	recall	F ₁ -score	specificity	accuracy
51	0.044478	0.710544	1.0	0.830781	0.782757	0.858315
52	0.046398	0.725117	1.0	0.840658	0.797840	0.868152
53	0.049362	0.740752	1.0	0.851071	0.813363	0.878276
54	0.052883	0.756430	1.0	0.861327	0.828285	0.888008
55	0.053363	0.773131	1.0	0.872052	0.843513	0.897940
56	0.056369	0.790504	1.0	0.882996	0.858673	0.907827
57	0.060077	0.809227	1.0	0.894556	0.874281	0.918007
58	0.066410	0.828651	1.0	0.906297	0.889728	0.928081
59	0.081708	0.849439	1.0	0.918591	0.905478	0.938353
60	0.084467	0.869931	1.0	0.930442	0.920266	0.947998
61	0.098710	0.892116	1.0	0.942982	0.935510	0.957940
62	0.101801	0.915615	1.0	0.955949	0.950852	0.967946
63	0.117203	0.940660	1.0	0.969423	0.966359	0.978060
64	0.117517	0.966909	1.0	0.983176	0.981749	0.988097
65	0.120692	0.993855	1.0	0.996918	0.996703	0.997850
66	0.305324	1.0	0.977596	0.988671	1.0	0.992208
67	0.305671	1.0	0.948721	0.973686	1.0	0.982165
68	0.305921	1.0	0.920021	0.958345	1.0	0.972183
69	0.306270	1.0	0.891253	0.942500	1.0	0.962177
70	0.306705	1.0	0.862537	0.926196	1.0	0.952190
71	0.307026	1.0	0.833867	0.909409	1.0	0.942219
72	0.307326	1.0	0.805069	0.892009	1.0	0.932202
73	0.307718	1.0	0.776369	0.874108	1.0	0.922220
74	0.308059	1.0	0.747593	0.855568	1.0	0.912212
75	0.308449	1.0	0.718748	0.836363	1.0	0.902180
76	0.308957	1.0	0.689980	0.816554	1.0	0.892174
77	0.310452	1.0	0.661234	0.796076	1.0	0.882176
78	0.312662	1.0	0.632534	0.774911	1.0	0.872194
79	0.313046	1.0	0.603788	0.752953	1.0	0.862196
80	0.313664	1.0	0.575050	0.730199	1.0	0.852201
81	0.316172	1.0	0.546297	0.706587	1.0	0.842201
82	0.317073	1.0	0.517521	0.682061	1.0	0.832192
83	0.320032	1.0	0.488798	0.656634	1.0	0.822202
84	0.320922	1.0	0.466833	0.636519	1.0	0.814563
85	0.320926	1.0	0.432193	0.603540	1.0	0.802515
86	0.320967	1.0	0.402402	0.573875	1.0	0.792154
87	0.321086	1.0	0.373489	0.543855	1.0	0.782098
88	0.321163	1.0	0.345032	0.513046	1.0	0.772200
89	0.321251	1.0	0.316657	0.481002	1.0	0.762331
90	0.321349	1.0	0.287464	0.446559	1.0	0.752178
91	0.321493	1.0	0.258787	0.411169	1.0	0.742204
92	0.322034	1.0	0.230026	0.374018	1.0	0.732201
93	0.323296	1.0	0.201265	0.335089	1.0	0.722198
94	0.324078	1.0	0.172535	0.294294	1.0	0.712205
95	0.325454	1.0	0.143721	0.251322	1.0	0.702184
96	0.325955	1.0	0.115059	0.206372	1.0	0.692215
97	0.326316	1.0	0.086260	0.158820	1.0	0.682198
98	0.326627	1.0	0.057567	0.108867	1.0	0.672219
99	0.326864	1.0	0.028738	0.055871	1.0	0.662192
100	1.294590	0.0	0.0	0.0	1.0	0.652197

Table A2 Performance metrics at different percentiles of reconstruction errors, demonstrating the trade-offs, and supporting the selection of the 67th percentile as the optimal threshold for anomaly detection with 90s resampling data.

Percentile	Optimal Threshold	precision	recall	F ₁ -score	specificity	accuracy
1	0.006183	0.328163	1.0	0.494161	0.014839	0.334894
2	0.007279	0.331551	1.0	0.497993	0.029824	0.345010
3	0.008931	0.334971	1.0	0.501840	0.044641	0.355014
4	0.009157	0.338433	1.0	0.505715	0.059334	0.364934
5	0.009793	0.342001	1.0	0.509688	0.074169	0.374949
6	0.010017	0.345617	1.0	0.513693	0.088892	0.384889
7	0.010216	0.349458	1.0	0.517923	0.104194	0.395219
8	0.010680	0.353281	1.0	0.522110	0.119094	0.405279
9	0.011087	0.357282	1.0	0.526467	0.134349	0.415578
10	0.011549	0.361237	1.0	0.530748	0.149093	0.425532
11	0.011866	0.365266	1.0	0.535084	0.163790	0.435454
12	0.011926	0.369464	1.0	0.539574	0.178757	0.445559
13	0.012397	0.373673	1.0	0.544049	0.193428	0.455464
14	0.012918	0.377979	1.0	0.548599	0.208099	0.465368
15	0.013253	0.382510	1.0	0.553356	0.223179	0.475549
16	0.013569	0.386962	1.0	0.557999	0.237653	0.485321
17	0.014060	0.391588	1.0	0.562793	0.252343	0.495238
18	0.014642	0.396336	1.0	0.567680	0.267065	0.505178
19	0.015152	0.401312	1.0	0.572766	0.282119	0.515341
20	0.015383	0.406249	1.0	0.577777	0.296692	0.525180
21	0.016471	0.411359	1.0	0.582926	0.311407	0.535114
22	0.016972	0.416781	1.0	0.588349	0.326625	0.545388
23	0.017516	0.422152	1.0	0.593681	0.341314	0.555305
24	0.018733	0.427626	1.0	0.599073	0.355905	0.565156
25	0.019276	0.433480	1.0	0.604794	0.371102	0.575415
26	0.019818	0.439228	1.0	0.610366	0.385631	0.585224
27	0.020752	0.445244	1.0	0.616151	0.400433	0.595218
28	0.021397	0.451311	1.0	0.621936	0.414962	0.605027
29	0.021789	0.457673	1.0	0.627950	0.429783	0.615033
30	0.022994	0.464117	1.0	0.633989	0.444381	0.624888
31	0.023402	0.470948	1.0	0.640332	0.459421	0.635042
32	0.023835	0.477815	1.0	0.646651	0.474107	0.644957
33	0.024215	0.484927	1.0	0.653132	0.488876	0.654928
34	0.024861	0.492325	1.0	0.659810	0.503788	0.664995
35	0.025308	0.499811	1.0	0.666498	0.518427	0.674878
36	0.026076	0.507678	1.0	0.673456	0.533346	0.684950
37	0.027332	0.515961	1.0	0.680705	0.548564	0.695225
38	0.027971	0.524266	1.0	0.687893	0.563337	0.705198
39	0.028229	0.532976	1.0	0.695348	0.578337	0.715325
40	0.028868	0.541850	1.0	0.702857	0.593124	0.725308
41	0.030642	0.551010	1.0	0.710517	0.607887	0.735275
42	0.032440	0.560660	1.0	0.718491	0.622919	0.745424
43	0.033150	0.570766	1.0	0.726736	0.638115	0.755683
44	0.034302	0.580823	1.0	0.734836	0.652714	0.765539
45	0.035420	0.591328	1.0	0.743188	0.667432	0.775475
46	0.036268	0.602303	1.0	0.751796	0.682260	0.785486
47	0.037056	0.613504	1.0	0.760462	0.696848	0.795335
48	0.037971	0.625625	1.0	0.769704	0.712044	0.805594
49	0.040528	0.638043	1.0	0.779031	0.727014	0.815701
50	0.043400	0.650496	1.0	0.788243	0.741452	0.825448

Table A2 Cont.

Percentile	Optimal Threshold	precision	recall	F ₁ -score	specificity	accuracy
51	0.045826	0.663835	1.0	0.797958	0.756317	0.835483
52	0.048199	0.677659	1.0	0.807863	0.771104	0.845467
53	0.050456	0.692141	1.0	0.818065	0.785962	0.855498
54	0.052603	0.707160	1.0	0.828463	0.800728	0.865466
55	0.054454	0.722501	1.0	0.838897	0.815177	0.875221
56	0.059021	0.739263	1.0	0.850087	0.830278	0.885417
57	0.059345	0.756508	1.0	0.861378	0.845117	0.895435
58	0.061814	0.774042	1.0	0.872631	0.859526	0.905162
59	0.062266	0.792979	1.0	0.884538	0.874372	0.915185
60	0.063552	0.813056	1.0	0.896890	0.889357	0.925302
61	0.064624	0.834007	1.0	0.909492	0.904225	0.935340
62	0.066418	0.856123	1.0	0.922485	0.919129	0.945402
63	0.071635	0.879033	1.0	0.935623	0.933779	0.955293
64	0.080885	0.903258	1.0	0.949170	0.948461	0.965205
65	0.081862	0.928700	1.0	0.963032	0.963056	0.975058
66	0.083409	0.956018	1.0	0.977515	0.977862	0.985054
67	0.092559	0.984360	1.0	0.992119	0.992354	0.994838
68	0.247001	1.0	0.984945	0.992416	1.0	0.995109
69	0.247376	1.0	0.954177	0.976551	1.0	0.985113
70	0.247714	1.0	0.923385	0.960167	1.0	0.975110
71	0.248124	1.0	0.892670	0.943292	1.0	0.965131
72	0.248636	1.0	0.861909	0.925833	1.0	0.955137
73	0.249020	1.0	0.831072	0.907743	1.0	0.945119
74	0.249385	1.0	0.800288	0.889067	1.0	0.935118
75	0.249814	1.0	0.769550	0.869769	1.0	0.925132
76	0.250269	1.0	0.738720	0.849729	1.0	0.915117
77	0.250836	1.0	0.708035	0.829064	1.0	0.905148
78	0.251605	1.0	0.677221	0.807551	1.0	0.895137
79	0.253747	1.0	0.646392	0.785222	1.0	0.885121
80	0.255437	1.0	0.615608	0.762076	1.0	0.875120
81	0.256051	1.0	0.584832	0.738036	1.0	0.865122
82	0.258708	1.0	0.554063	0.713051	1.0	0.855126
83	0.259548	1.0	0.523325	0.687082	1.0	0.845140
84	0.261897	1.0	0.492457	0.659928	1.0	0.835112
85	0.263021	1.0	0.461757	0.631784	1.0	0.825138
86	0.263048	1.0	0.430829	0.602209	1.0	0.815090
87	0.263070	1.0	0.400455	0.571892	1.0	0.805222
88	0.263121	1.0	0.369103	0.539189	1.0	0.795037
89	0.263373	1.0	0.338592	0.505892	1.0	0.785124
90	0.263605	1.0	0.307823	0.470741	1.0	0.775128
91	0.263857	1.0	0.276766	0.433543	1.0	0.765039
92	0.264606	1.0	0.246240	0.395173	1.0	0.755122
93	0.265771	1.0	0.215487	0.354568	1.0	0.745131
94	0.266736	1.0	0.184703	0.311813	1.0	0.735130
95	0.268147	1.0	0.153896	0.266742	1.0	0.725121
96	0.268774	1.0	0.123112	0.219234	1.0	0.715121
97	0.269189	1.0	0.092306	0.169011	1.0	0.705112
98	0.269561	1.0	0.061568	0.115994	1.0	0.695126
99	0.269839	1.0	0.030708	0.059586	1.0	0.685101
100	1.137619	1.0	0.000030	0.000061	1.0	0.675071

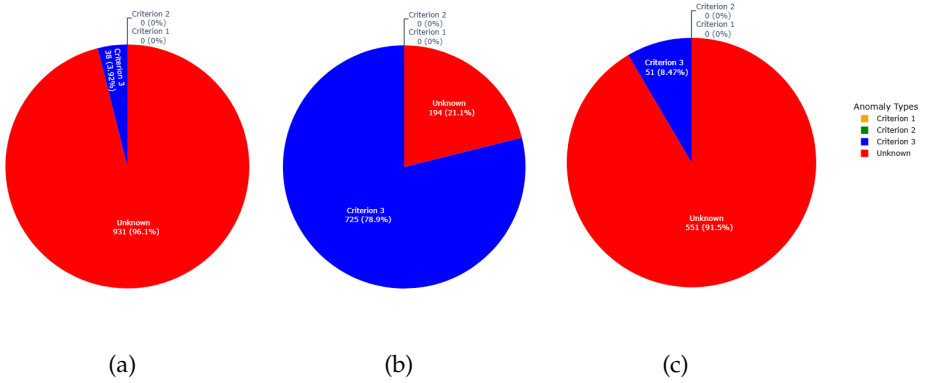


Figure B1 (a) False anomaly distribution for without sampling, (b) false anomaly distribution for 90s sampling interval, and (c) false anomaly distribution for 65s sampling interval.

positioned receiver (Criterion 3). The results show that some false anomalies closely resembled true anomalies falling under type *a fish passing more than one consecutively positioned receiver*, while others did not resemble any of the predefined criteria.

Appendix C

Performance comparison of classifiers without resampling and with resampling at 90s and 65s intervals. Metrics evaluated include accuracy, recall, specificity, precision, F_1 -score, AUC, and the number of parameters and training time, as shown in Table C4. A visual representation of these metrics is provided in Figure C2.

Table A3 Performance metrics at different percentiles of reconstruction errors, demonstrating the trade-offs, and supporting the selection of the 69th percentile as the optimal threshold for anomaly detection with 65s resampling data.

Percentile	Optimal Threshold	precision	recall	F ₁ -score	specificity	accuracy
1.0	0.006671	0.307389	1.0	0.470234	0.014377	0.314317
2.0	0.010666	0.310526	1.0	0.473895	0.028751	0.324317
3.0	0.012341	0.313727	1.0	0.477614	0.043125	0.334317
4.0	0.012690	0.316995	1.0	0.481391	0.057499	0.344317
5.0	0.014052	0.320332	1.0	0.485229	0.071873	0.354316
6.0	0.014491	0.323739	1.0	0.489129	0.086247	0.364315
7.0	0.015116	0.327220	1.0	0.493091	0.100621	0.374315
8.0	0.015249	0.330777	1.0	0.497119	0.114995	0.384315
9.0	0.016012	0.334412	1.0	0.501212	0.129369	0.394315
10.0	0.016358	0.338128	1.0	0.505375	0.143746	0.404317
11.0	0.016491	0.341927	1.0	0.509606	0.158120	0.414316
12.0	0.017035	0.345813	1.0	0.513909	0.172494	0.424316
13.0	0.017731	0.349788	1.0	0.518285	0.186868	0.434316
14.0	0.018500	0.353855	1.0	0.522737	0.201242	0.444316
15.0	0.019028	0.358018	1.0	0.527265	0.215615	0.454316
16.0	0.020337	0.362280	1.0	0.531873	0.229989	0.464315
17.0	0.020939	0.366644	1.0	0.536561	0.244363	0.474315
18.0	0.021852	0.371115	1.0	0.541334	0.258737	0.484315
19.0	0.022952	0.375698	1.0	0.546193	0.273114	0.494317
20.0	0.023814	0.380394	1.0	0.551139	0.287488	0.504316
21.0	0.024190	0.385209	1.0	0.556175	0.301862	0.514316
22.0	0.024612	0.390148	1.0	0.561304	0.316236	0.524316
23.0	0.024765	0.395214	1.0	0.566529	0.330610	0.534315
24.0	0.025395	0.400414	1.0	0.571851	0.344984	0.544316
25.0	0.026067	0.405753	1.0	0.577275	0.359358	0.554315
26.0	0.026479	0.411236	1.0	0.582803	0.373732	0.564315
27.0	0.027067	0.416869	1.0	0.588437	0.388106	0.574315
28.0	0.027698	0.422660	1.0	0.594183	0.402483	0.584316
29.0	0.028432	0.428613	1.0	0.600041	0.416857	0.594316
30.0	0.028545	0.434736	1.0	0.606015	0.431231	0.604316
31.0	0.028979	0.441036	1.0	0.612110	0.445605	0.614315
32.0	0.030082	0.447522	1.0	0.618328	0.459979	0.624315
33.0	0.030927	0.454201	1.0	0.624675	0.474353	0.634315
34.0	0.032055	0.461083	1.0	0.631152	0.488727	0.644315
35.0	0.033005	0.468176	1.0	0.637766	0.503100	0.654315
36.0	0.033521	0.475491	1.0	0.644519	0.517474	0.664315
37.0	0.033939	0.483040	1.0	0.651419	0.531852	0.674316
38.0	0.034578	0.490831	1.0	0.658466	0.546226	0.684316
39.0	0.036113	0.498877	1.0	0.665668	0.560599	0.694316
40.0	0.036358	0.507192	1.0	0.673029	0.574973	0.704316
41.0	0.036784	0.515788	1.0	0.680554	0.589347	0.714315
42.0	0.036888	0.524681	1.0	0.688250	0.603721	0.724315
43.0	0.037256	0.533885	1.0	0.696122	0.618095	0.734315
44.0	0.037454	0.543419	1.0	0.704175	0.632469	0.744315
45.0	0.037617	0.553299	1.0	0.712418	0.646843	0.754314
46.0	0.038178	0.563547	1.0	0.720857	0.661220	0.764316
47.0	0.039061	0.574180	1.0	0.729497	0.675594	0.774316
48.0	0.039714	0.585221	1.0	0.738347	0.689968	0.784316
49.0	0.040355	0.596696	1.0	0.747413	0.704342	0.794315
50.0	0.041110	0.608630	1.0	0.756706	0.718716	0.804315

Table A3 Cont.

Percentile	Optimal Threshold	precision	recall	F1-score	specificity	accuracy
51	0.041448	0.621665	1.0	0.766699	0.733786	0.814799
52	0.041923	0.634732	1.0	0.776558	0.748272	0.824877
53	0.042794	0.648075	1.0	0.786463	0.762461	0.834747
54	0.043785	0.662063	1.0	0.796677	0.776722	0.844669
55	0.045243	0.676877	1.0	0.807307	0.791182	0.854728
56	0.046965	0.692268	1.0	0.818154	0.805549	0.864724
57	0.047245	0.708431	1.0	0.829335	0.819966	0.874753
58	0.049649	0.725328	1.0	0.840800	0.834350	0.884760
59	0.053066	0.743171	1.0	0.852666	0.848830	0.894833
60	0.058090	0.761818	1.0	0.864809	0.863237	0.904856
61	0.065950	0.780976	1.0	0.877020	0.877323	0.914655
62	0.072420	0.801347	1.0	0.889720	0.891561	0.924561
63	0.075440	0.822972	1.0	0.902891	0.905905	0.934540
64	0.076202	0.845608	1.0	0.916346	0.920133	0.944438
65	0.077088	0.869489	1.0	0.930189	0.934341	0.954322
66	0.082129	0.895779	1.0	0.945025	0.949106	0.964594
67	0.084271	0.922321	1.0	0.959591	0.963159	0.974370
68	0.091506	0.950524	1.0	0.974634	0.977231	0.984160
69	0.098479	0.981761	1.0	0.990797	0.991873	0.994346
70	0.206688	1.0	0.985892	0.992896	1.0	0.995707
71	0.207152	1.0	0.952980	0.975924	1.0	0.985691
72	0.207554	1.0	0.920135	0.958406	1.0	0.975696
73	0.208043	1.0	0.887214	0.940237	1.0	0.965678
74	0.208644	1.0	0.854355	0.921458	1.0	0.955678
75	0.209169	1.0	0.821548	0.902033	1.0	0.945694
76	0.209650	1.0	0.788658	0.881843	1.0	0.935685
77	0.210060	1.0	0.755806	0.860922	1.0	0.925688
78	0.210598	1.0	0.722908	0.839172	1.0	0.915677
79	0.211333	1.0	0.690109	0.816644	1.0	0.905695
80	0.213318	1.0	0.657211	0.793153	1.0	0.895684
81	0.213755	1.0	0.624253	0.768665	1.0	0.885655
82	0.213862	1.0	0.591522	0.743341	1.0	0.875694
83	0.214154	1.0	0.558601	0.716798	1.0	0.865676
84	0.214395	1.0	0.525628	0.689064	1.0	0.855642
85	0.215216	1.0	0.492844	0.660275	1.0	0.845665
86	0.215768	1.0	0.460151	0.630278	1.0	0.835716
87	0.216072	1.0	0.427071	0.598528	1.0	0.825649
88	0.216426	1.0	0.394302	0.565591	1.0	0.815677
89	0.217883	1.0	0.361465	0.530995	1.0	0.805684
90	0.220101	1.0	0.328583	0.494637	1.0	0.795678
91	0.221149	1.0	0.295753	0.456496	1.0	0.785687
92	0.222492	1.0	0.262894	0.416335	1.0	0.775688
93	0.223228	1.0	0.230041	0.374038	1.0	0.765690
94	0.223757	1.0	0.197159	0.329378	1.0	0.755683
95	0.224262	1.0	0.164329	0.282273	1.0	0.745693
96	0.225074	1.0	0.131416	0.232304	1.0	0.735677
97	0.226338	1.0	0.098602	0.179505	1.0	0.725691
98	0.227912	1.0	0.065682	0.123267	1.0	0.715673
99	0.231056	1.0	0.032867	0.063643	1.0	0.705687
100	1.103892	0.0	0.0	0.0	1.0	0.695685

Table C4 Performance comparison of classifiers without resampling and with resampling at 90s and 65s intervals. Metrics evaluated include accuracy, recall, specificity, precision, F₁-score, AUC, and the number of parameters and training time.

Classifiers Resampling	IF			DBSCAN			LOF			NN-AE		
	NO	90s	65s	NO	90s	65s	NO	90s	65s	NO	90s	65s
Accuracy	67.60±0.0011	67.61± 0.0012	67.62±0.0012	66.00±0.0011	66.00±0.0012	66.00±0.0012	66.83±0.0013	66.83±0.0012	66.83±0.0013	99.76±0.0013	99.77±0.0002	99.85±0.0002
Recall	0.10±0.0001	0.15± 0.0002	0.16± 0.0002	0.24±0.0002	0.24±0.0002	0.24±0.0002	0.40±0.0003	0.40±0.0003	0.40±0.0003	100±0.0000	100±0.0000	100±0.0000
Specificity	100±0.0000	100±0.0000	100±0.0000	97.57±0.0002	97.57±0.0005	97.57±0.0004	98.71±0.0004	98.71±0.0003	98.71±0.0003	99.64±0.0002	99.66±0.0003	99.78±0.0003
Precision	100±0.0000	100±0.0000	100±0.0000	4.69±0.0036	4.69±0.0040	4.69±0.0040	13.16±0.0092	13.16±0.0091	13.16±0.0084	99.27±0.0092	99.31±0.0005	99.55±0.0006
F ₁ -score	0.21±0.0003	0.30±0.0003	0.33±0.0004	0.47±0.0004	0.47±0.0004	0.47±0.0005	0.78±0.0006	0.78±0.0005	0.78±0.0006	99.63±0.0005	99.65±0.0002	99.77±0.0003
AUC	50.05±0.0001	50.07±0.0001	50.08±0.0001	48.90±0.0003	48.90±0.0003	48.90±0.0002	49.56±0.0003	49.56±0.0002	49.56±0.0002	99.82±0.0001	99.83±0.0001	99.89±0.0001
No. of parameters	5	5	5	2	2	2	5	5	5	3597	3597	3597
Train time (minutes)	4.17	4.55	4.74	8.92	9.13	9.44	24.61	26.73	32.48	699.65	737.97	852.87

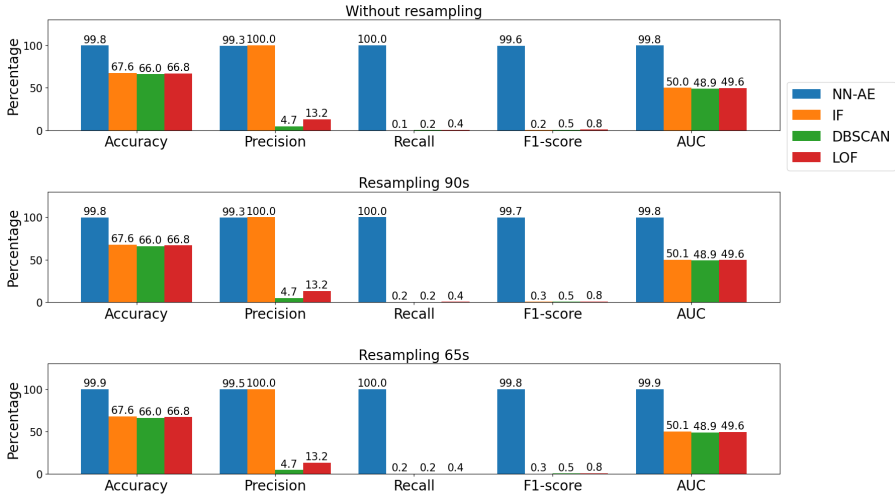


Figure C2 This bar chart shows the key performance metrics (Precision, Recall, Accuracy, F1-score, and AUC) for different models (NN-AE, IF, DBSCAN, LOF) evaluated on data without resampling, with 90s resampling, and with 65s resampling. The NN-AE model consistently achieves near-perfect performance, significantly outperforming the traditional models.

Appendix D

Figures [D3](#), [D4](#), [D5](#), and [D6](#) illustrate the movement patterns of adult dusky kob in the Breede Estuary, highlighting anomalies and TA as detected by the NN-AE, IF, LOF, and DBSCAN algorithms. Each figure consists of two parts: (a) provides an overview of dusky kob movements from 2016 to 2021, represented by blue lines indicating latitudinal shifts over time. Red dots denote anomalies and magenta crosses indicate TA, where the models correctly identified unusual movements.

At the top of each panel (a), a black square zoomed a specific region that focuses on a particular time frame in 2020. This region is examined in more detail in panel (b) of each figure, which zooms in on fish movements during this period. The zoomed-in view provides a granular analysis of daily or monthly fish movements, enabling a closer evaluation of how each model performs in detecting anomalies. By narrowing the focus to this specific interval, the detailed visualization helps assess the models' precision and accuracy in identifying TA, offering insights into their reliability and effectiveness in capturing significant behavioural deviations.

Figure [D7](#) compares the performance of the NN-AE, IF, DBSCAN, and LOF models in FA. Panel (b) of Figure [D7](#) shows that the IF model does not produce any FA, while NN-AE generates the fewest FA among the remaining models, followed by LOF and DBSCAN. This indicates that IF is the most effective in avoiding the misclassification of normal behaviours as anomalies.

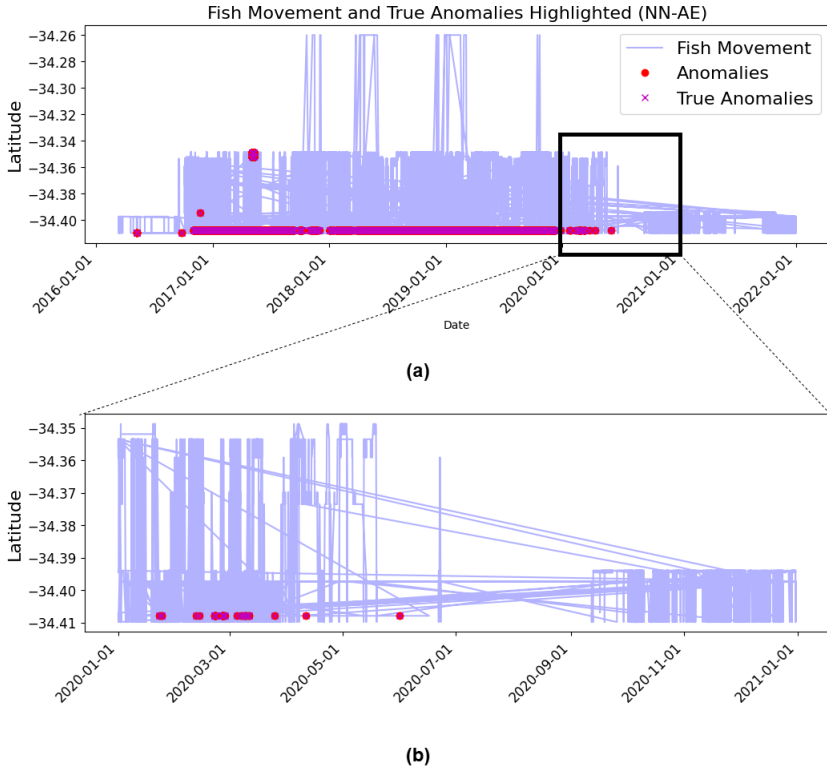


Figure D3 This figure shows the movement patterns of dusky kob in the Breede Estuary from 2016 to 2021, with a focus on highlighting anomalies and TA detected by the NN-AE. (a) An overview from 2016 to 2021, with blue lines indicating latitudinal movements, red dots highlighting anomalies, and magenta crosses marking TA. (b) A zoomed-in view of the 2020 movement patterns, shows a closer examination of anomalies and TA.

However, the absence of FA does not necessarily make IF the best overall model. While NN-AE produces slightly more FA than IF, it achieves 100% of TA with negligible FA. NN-AE's capacity to learn complex spatial and temporal patterns enables it to identify meaningful anomalies that reflect significant changes in fish behaviour or environmental conditions, without overrepresenting irrelevant data. This capability positions NN-AE as the most suitable model for anomaly detection in telemetry data.

Figure D8 compares fish movement data over time, highlighting anomalies and FN detections. Each plot visualizes the changes in fish latitude from 2016 to 2021, with anomalies marked in red and FN in green. NN-AE model (a) achieves zero FN demonstrating its exceptional accuracy in detecting anomalies. This superior performance is attributed to the model's ability to learn complex temporal and spatial patterns in the fish movement data. The absence of FN indicates that NN-AE effectively identifies all anomalies in the telemetry observation. This capability is particularly valuable for telemetry

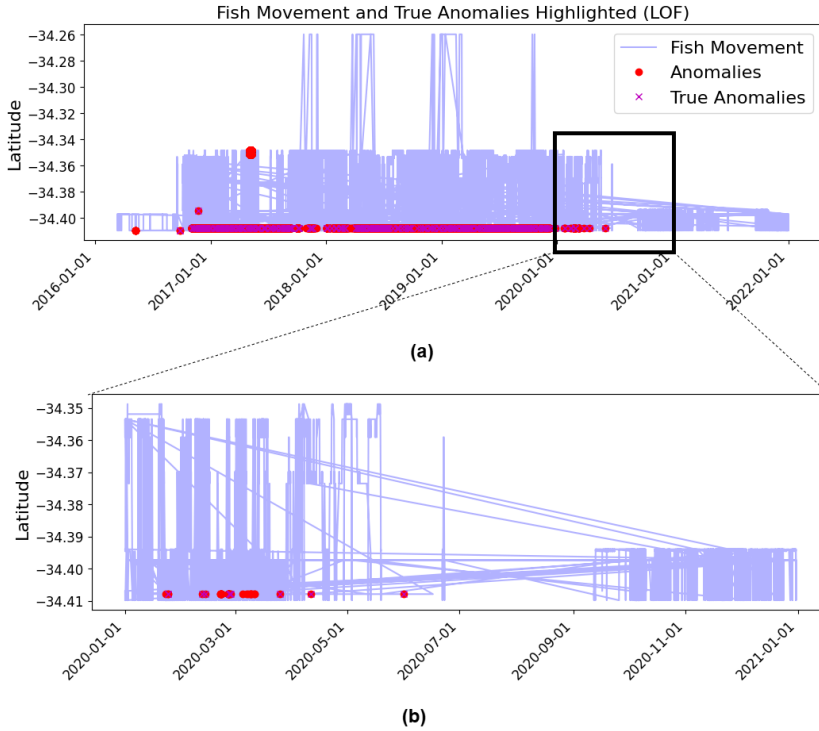


Figure D4 This figure shows the movement patterns of dusky kob in the Breede Estuary from 2016 to 2021, with a focus on highlighting anomalies and TA detected by the LOF. (a) An overview from 2016 to 2021, with blue lines indicating latitudinal movements, red dots highlighting anomalies, and magenta crosses marking TA. (b) A zoomed-in view of the 2020 movement patterns, shows a closer examination of anomalies and TA.

research, as removing anomalies could provides a more complete understanding of the factors influencing fish movement. In contrast, the IF (b), DBSCAN (c), and LOF (d) models misclassify a significant number of anomalies as normal instances, which undermines their effectiveness in detecting true behavioural anomalies.

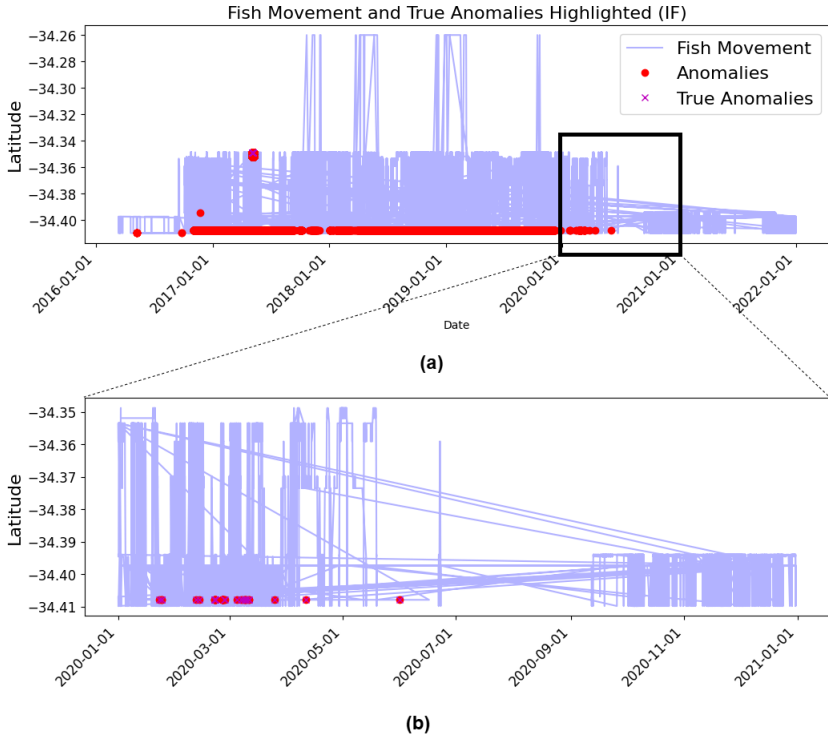


Figure D5 This figure shows the movement patterns of dusky kob in the Breede Estuary from 2016 to 2021, with a focus on highlighting anomalies and TA detected by the IF. (a) An overview from 2016 to 2021, with blue lines indicating latitudinal movements, red dots highlighting anomalies, and magenta crosses marking TA. (b) A zoomed-in view of the 2020 movement patterns, shows a closer examination of anomalies and TA.

References

- [1] Crossin, G.T., Heupel, M.R., Holbrook, C.M., Hussey, N.E., Lowerre-Barbieri, S.K., Nguyen, V.M., Raby, G.D., Cooke, S.J.: Acoustic telemetry and fisheries management. *Ecological Applications* **27**(4), 1031–1049 (2017)
- [2] Lowerre-Barbieri, S.K., Kays, R., Thorson, J.T., Wikelski, M.: The ocean’s movescape: fisheries management in the bio-logging decade (2018–2028). *ICES Journal of Marine Science* **76**(2), 477–488 (2019)
- [3] Hughes, J.M., Meadows, N.M., Stewart, J., Booth, D.J., Fowler, A.M.: Movement patterns of an iconic recreational fish species, mullet (*argyrosomus japonicus*), revealed by cooperative citizen-science tagging programs in coastal eastern Australia. *Fisheries Research* **247**, 106179 (2022)
- [4] Thorstad, E.B., Rikardsen, A.H., Alp, A., Okland, F.: The use of electronic

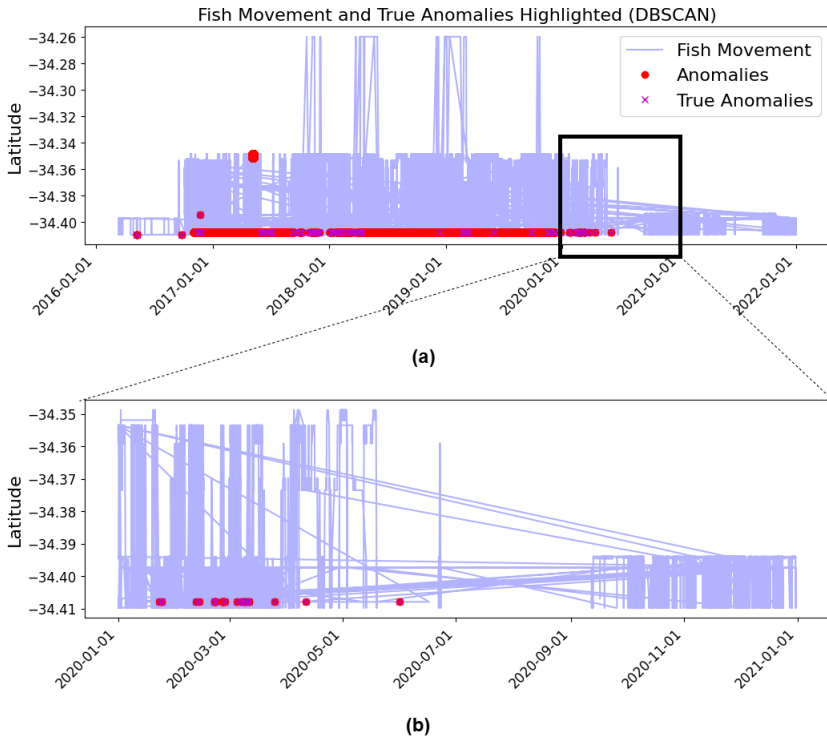
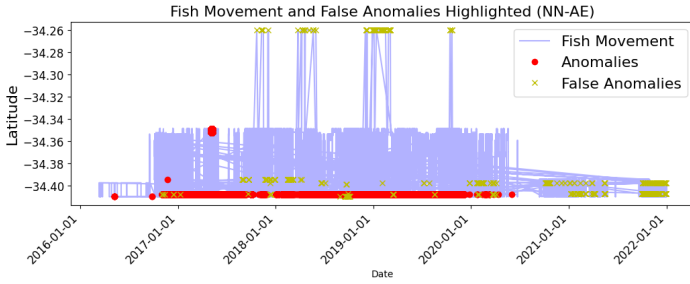


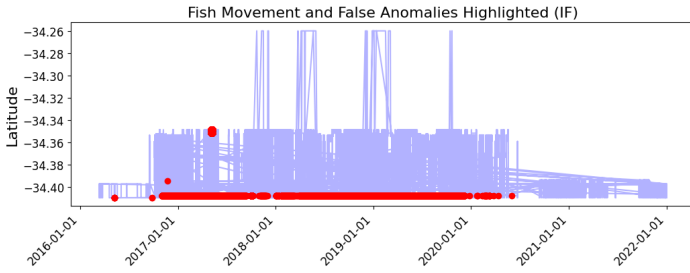
Figure D6 This figure shows the movement patterns of dusky kob in the Breede Estuary from 2016 to 2021, with a focus on highlighting anomalies and TA detected by the DBSCAN. (a) An overview from 2016 to 2021, with blue lines indicating latitudinal movements, red dots highlighting anomalies, and magenta crosses marking TA. (b) A zoomed-in view of the 2020 movement patterns, shows a closer examination of anomalies and TA.

tags in fish research - an overview of fish telemetry methods. *Turkish Journal of Fisheries and Aquatic Sciences* **13**, 881–896 (2013)

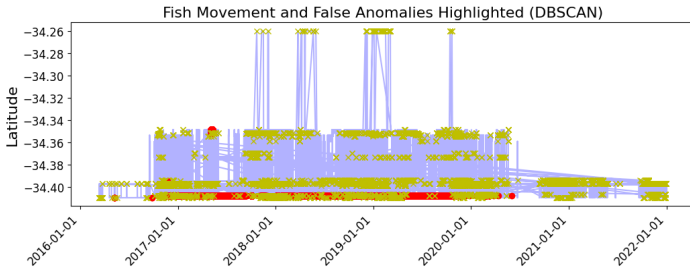
- [5] Hussey, N.E., Kessel, S.T., Aaerstrup, K., Cooke, S.J., Cowley, P.D., Fisk, A.T., Harcourt, R.G., Holland, K.N., Iverson, S.J., Kocik, J.F., Mills Fleming, J.E., Whoriskey, F.G.: Aquatic animal telemetry: a panoramic window into the underwater world. *Science* **348**, 1255642 (2015)
- [6] Matley, J.K., Kilnard, N.V., Barbosa Martins, A.P., Aaerstrup, K., Aspillaga, E., Cooke, S.J., Cowley, P.D., Heupel, M.R., Lowe, C.G., Lowerre-Barbieri, S.K., Mitamura, H., Moore, J.-S., Simpfendorfer, C.A., Stokesbury, M.J.W., Taylor, M.D., Thorstad, E.B., vandergoot, C.S., Fisk, A.T.: Global trends in aquatic animal tracking with acoustic telemetry. *Trends in Ecology and Evolution* **37**(1), 79–94 (2022)
- [7] Dhellemmes, F., Aspillaga, E., Monk, C.T.: Atfilter: A solution for managing and filtering detections from passive acoustic telemetry data. *MethodsX* **10**, 102222 (2023)



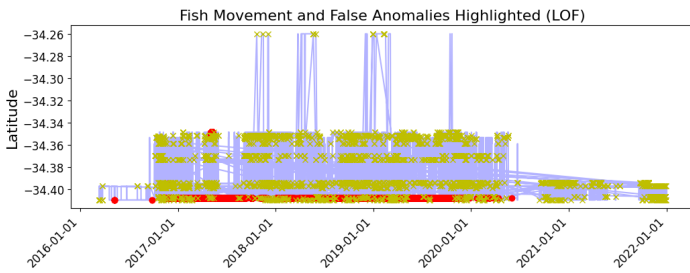
(a)



(b)

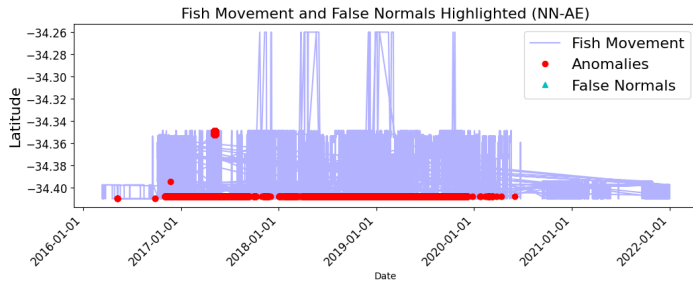


(c)

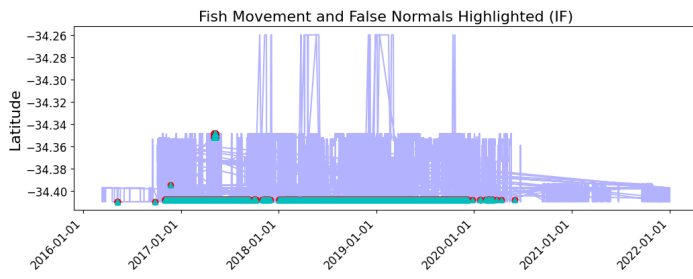


(d)

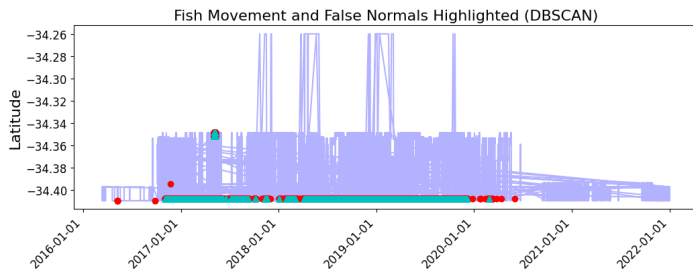
Figure D7 This figure shows the movement patterns of dusky kob in the Breede Estuary from 2016 to 2021, highlighting anomalies and FA detected by four machine learning models: NN-AE (a), IF (b), DBSCAN (c), and LOF (d). Blue lines represent fish movements, red dots indicate unusual movement patterns (anomalies) and magenta crosses mark correctly identified FA.



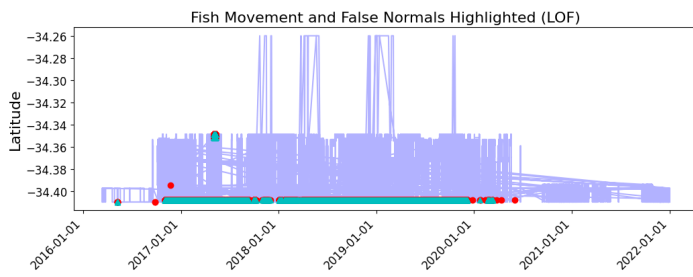
(a)



(b)

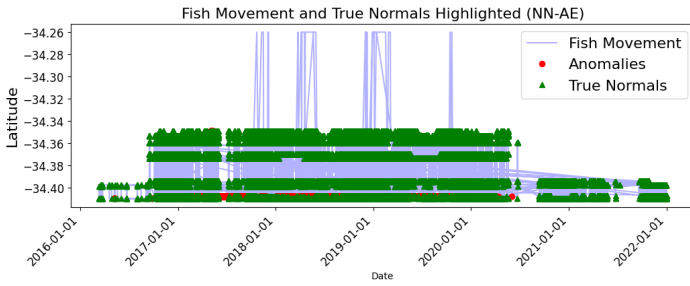


(c)

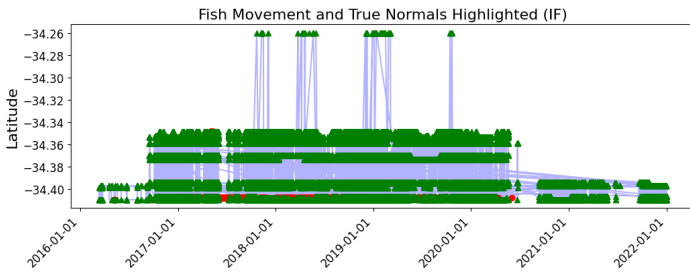


(d)

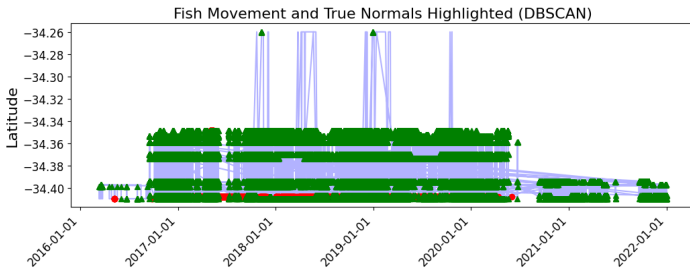
Figure D8 This figure shows the movement patterns of dusky kob in the Breede Estuary from 2016 to 2021, highlighting anomalies and FN detected by four machine learning models: NN-AE (a), IF (b), DBSCAN (c), and LOF (d). Blue lines represent fish movements, red dots indicate unusual movement patterns (anomalies) and magenta crosses mark correctly identified FN.



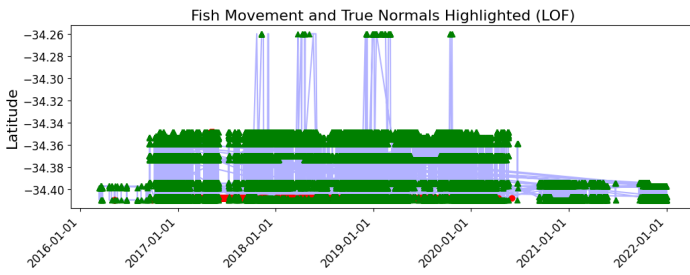
(a)



(b)



(c)



(d)

Figure D9 This figure shows the movement patterns of dusky kob in the Breede Estuary from 2016 to 2021, highlighting anomalies and TN detected by four machine learning models: NN-AE (a), IF (b), DBSCAN (c), and LOF (d). Blue lines represent fish movements, red dots indicate unusual movement patterns (anomalies) and magenta crosses mark correctly identified TN.

- [8] Simpfendorfer, C.A., Huveneers, A. Charlie; Steckenreuter, Tattersll, X. Katherine; Hoenner, Harcourt, R., Heupel, M.R.: Ghosts in the data: false detections in vemco pulse position modulation acoustic telemetry monitoring equipment. *Animal Biotelemetry* **3**(55), 40317–0150094 (2015)
- [9] Chambert, T., Miller, D.A.W., Nichols, J.D.: Modeling false positive detections in species occurrence data under different study designs. *Ecology* **96**, 332–339 (2015)
- [10] R Core Team: R: A Language and Environment for Statistical Computing. R Foundation for Statistical Computing, Vienna, Austria (2022). R Foundation for Statistical Computing. <https://www.R-project.org/>
- [11] Flávio, H., Baktoft, H., Codling, E.: actel: Standardised analysis of acoustic telemetry data from animals moving through receiver arrays. *Methods in Ecology & Evolution* **12**(1) (2021)
- [12] Niella, Y., Flávio, H., Smoothey, A.F., Aarestrup, K., Taylor, M.D., Peddemors, V.M., Harcourt, R.: Refined shortest paths (rsp): Incorporation of topography in space use estimation from node-based telemetry data. *Methods in Ecology and Evolution* **11**(12), 1733–1742 (2020)
- [13] Spaulding, T.: telemetR: Filter and Analyze Generalised Telemetry Data from Organisms. (2024). R package version 1.0. <https://github.com/tspaulding-esa/telemetr>
- [14] Wu, Z., Zhang, C., Gu, X., Duporge, I., Hughey, L.F., Stabach, J.A., Skidmore, S.K., Hopcraft, J.G.C., Lee, S.J., Atkinson, P.M., McCauley, D.J., Lamprey, R., Ngene, S., Wang, T.: Deep learning enables satellite-based monitoring of large populations of terrestrial mammals across heterogenous landscape. *Nature Communications* **14**, 3072 (2023)
- [15] Wang, J.-H., Lee, S.-K., Lai, Y.-C., Lin, C.-C., Wang, T.-Y., Lin, Y.-R., Hsu, T.-H., Huang, C.-W., Chiang, C.-P.: Anomalous behaviors detection for underwater fish using ai techniques. *IEEE access* **8**, 224372–224382 (2020)
- [16] Notte, D.V., Lennox, R.J., Hardie, D.C., Crossin, G.T.: Application of machine learning and acoustic predation tags to classify migration fate of atlantic salmon smolts. *Oecologia* **198**, 605–618 (2022)
- [17] Klinard, V. Natalie, Matley, J.K., Ivanova, S.V., Larocque, S.M., Fisk, A.T., Johnson, T.B.: Application of machine learning to identify predators of stocked fish in lake ontario: using acoustic telemetry predation tags to inform management. *Journal of Fish Biology* **98**(1), 237–250 (2020)

- [18] Griffin, L.P., Casselberry, G.A., Hart, K.M., Jordaan, A., Becker, S.L., Novak, A.J., DeAngelis, B.M., Pollock, C.G., Lundgren, I., Hillis-Starr, Z., Danylchuk, A.J., Skomal, G.B.: A novel framework to predict relative habitat selection in aquatic systems: applying machine learning and resource selection functions to acoustic telemetry data from multiple shark species. *Frontiers in Marine Science* **8**, 631262 (2021)
- [19] Guénard, G., Morin, J., Matte, P., Secretan, Y., Valiquette, E., Mingelbier, M.: Deep learning habitat modeling for moving organisms in rapidly changing estuarine environments: a case of two fishes. *Estuarine, Coastal and Shelf Science* **238**, 106713 (2020)
- [20] Schindler, T.F., Schlicht, S., Thoben, K.-D.: Towards benchmarking for evaluating machine learning methods in detecting outliers in process datasets. *Computers* **12**(12), 253 (2023)
- [21] Chen, H., Liu, H., Chu, X., Liu, Q., Xue, D.: Anomaly detection and critical scada parameters identification for wind turbines based on lstm-ae neural network. *Renewable Energy* **172**, 829–840 (2021)
- [22] Benova, L., Hudec, L.: Comprehensive analysis and evaluation of anomalous user activity in web server logs. *Sensors* **24**(3), 746 (2024)
- [23] Ziko, B., Murray, T., Næsje, T., Filmalter, J., Cowley, P.: Acoustic telemetry reveals the drivers behind estuary–sea connectivity of an important estuarine-dependent fishery species, pomadasys commersonnii, in the breede estuary, south africa. *African Journal of Marine Science* **45**(3), 201–213 (2023)
- [24] Childs, A.-R., Cowley, P.D., Næsje, T.F., Bennett, R.H.: Habitat connectivity and intra-population structure of an estuary-dependent fishery species. *Marine Ecology Progress Series* **537**, 233–245 (2015)
- [25] Cowley, P.D., Kerwath, S., Næsje, T., Childs, A.-R., Gillespie, L.D., Leggitt, C., Thorstad, E.B., Økland, F.: Space use patterns and movements of juvenile dusky kob *argyrosomus japonicus* in the great fish estuary (south africa): implications for management. NINA rapport (2006)
- [26] Griffiths, M.H., Heemstra, P.C.: A contribution to the taxonomy of the marine fish genus *argyrosomus* (perciformes: Sciaenidae), with descriptions of two new species from southern africa. *Ichthyologica Bulletin JLB Smith Institute of Ichthyology* **65**, 1–40 (1995)
- [27] Griffiths, M.H.: Life history of the dusky kob *argyrosomus japonicus* (sciaenidae) off the east coast of south africa. *South African Journal of Marine Science* **17**, 135–154 (1996)

- [28] Ter Morhuizen, L.D., Whitfield, A.K., Paterson, A.W.: Influence of fresh-water flow regime on fish assemblages in the great fish river and estuary. *South African Journal of Aquatic Sciences* **22**, 52–61 (1996)
- [29] Cowley, P., Kerwath, S., Childs, A., Thorstad, E., Økland, F., Næsje, T.: Estuarine habitat use by juvenile dusky kob *argyrosomus japonicus* (sciaenidae), with implications for management. *African Journal of Marine Science* **30**(2), 247–253 (2008)
- [30] Næsje, T.F., Cowley, P.D., Diserud, O.H., Childs, A.-R., Kerwath, S.E., Thorstad, E.B.: Riding the tide: estuarine movements of a sciaenid fish, *argyrosomus japonicus*. *Marine Ecology Progress Series* **460**, 221–232 (2012)
- [31] Childs, A.-R.: Estuarine-dependency and multiple habitat use by dusky kob *argyrosomus japonicus* (pisces: Sciaenidae). PhD thesis, Rhodes University (2013)
- [32] MARCIUC, A.M.: Data preprocessing techniques. *BUILDING BRIDGES–INNOVATION, ENTREPRENEURSHIP AND SOCIETY*, 107 (2021)
- [33] Zheng, A., Casari, A.: Feature Engineering for Machine Learning: Principles and Techniques for Data Scientists. " O'Reilly Media, Inc.", ??? (2018)
- [34] Santhosh, A., Idicula, S.M.: Home range estimation of migrating organisms considering the spatiotemporal aspects of gps tracked data. In: 2017 International Conference of Electronics, Communication and Aerospace Technology (ICECA), vol. 1, pp. 162–167 (2017). IEEE
- [35] Liu, F.T., Ting, K.M., Zhou, Z.-H.: Isolation forest. In: 2008 Eighth Ieee International Conference on Data Mining, pp. 413–422 (2008). IEEE
- [36] Hariri, S., Kind, M.C., Brunner, R.J.: Extended isolation forest. *IEEE transactions on knowledge and data engineering* **33**(4), 1479–1489 (2019)
- [37] Breunig, M.M., Kriegel, H.-P., Ng, R.T., Sander, J.: Lof: identifying density-based local outliers. In: Proceedings of the 2000 ACM SIGMOD International Conference on Management of Data, pp. 93–104 (2000)
- [38] Alghushairy, O., Alsini, R., Soule, T., Ma, X.: A review of local outlier factor algorithms for outlier detection in big data streams. *Big Data and Cognitive Computing* **5**(1), 1 (2020)
- [39] Cheng, Z., Zou, C., Dong, J.: Outlier detection using isolation forest and

- local outlier factor. In: Proceedings of the Conference on Research in Adaptive and Convergent Systems, pp. 161–168 (2019)
- [40] Ester, M., Kriegel, H.-P., Sander, J., Xu, X., *et al.*: A density-based algorithm for discovering clusters in large spatial databases with noise. In: Kdd, vol. 96, pp. 226–231 (1996)
- [41] Khan, K., Rehman, S.U., Aziz, K., Fong, S., Sarasvady, S.: Dbscan: Past, present and future. In: The Fifth International Conference on the Applications of Digital Information and Web Technologies (ICADIWT 2014), pp. 232–238 (2014). IEEE
- [42] Schubert, E., Sander, J., Ester, M., Kriegel, H.P., Xu, X.: Dbscan revisited, revisited: why and how you should (still) use dbscan. *ACM Transactions on Database Systems (TODS)* **42**(3), 1–21 (2017)
- [43] Nwadiugwu, M.C.: Neural networks, artificial intelligence and the computational brain. arXiv preprint arXiv:2101.08635 (2020)
- [44] Hinton, G.E., Salakhutdinov, R.R.: Reducing the dimensionality of data with neural networks. *science* **313**(5786), 504–507 (2006)
- [45] Chen, Z., Yeo, C.K., Lee, B.S., Lau, C.T.: Autoencoder-based network anomaly detection. In: 2018 Wireless Telecommunications Symposium (WTS), pp. 1–5 (2018). IEEE
- [46] Sakurada, M., Yairi, T.: Anomaly detection using autoencoders with nonlinear dimensionality reduction. In: Proceedings of the MLSDA 2014 2nd Workshop on Machine Learning for Sensory Data Analysis, pp. 4–11 (2014)
- [47] Zahedi, L., Mohammadi, F.G., Rezapour, S., Ohland, M.W., Amini, M.H.: Search algorithms for automated hyper-parameter tuning. arXiv preprint arXiv:2104.14677 (2021)
- [48] ramlakhan: Difference Between Shallow and Deep Neural Networks. *Geek for Geeks*, (2024). *Geek for Geeks*. <https://www.geeksforgeeks.org/difference-between-shallow-and-deep-neural-networks/>